PROCEEDINGS A

royalsocietypublishing.org/journal/rspa

Research

Cite this article: Gower AL, Hawkins SC, Kristensson G. 2023 A model to validate effective waves in random particulate media: spherical symmetry. *Proc. R. Soc. A* **479**: 20230444.
https://doi.org/10.1098/rspa.2023.0444

Received: 19 June 2023
Accepted: 30 October 2023

Subject Areas:
applied mathematics, acoustics, wave motion

Keywords:
multiple scattering, random media, particulates, wave propagation, Monte Carlo validation

Author for correspondence:
Artur L. Gower
e-mail: arturgower@gmail.com

One contribution to a special feature 'Mathematical theory and applications of multiple wave scattering' organized by guest editors Luke G. Bennetts, Michael H. Meylan, Malte A. Peter, Valerie J. Pinfield and Olga Umnova.

THE ROYAL SOCIETY PUBLISHING

A model to validate effective waves in random particulate media: spherical symmetry

Artur L. Gower[1], Stuart C. Hawkins[2] and Gerhard Kristensson[3]

[1]Department of Mechanical Engineering, University of Sheffield, Sheffield, UK
[2]School of Mathematical and Physical Sciences, Macquarie University, Sydney, Australia
[3]Department of Electrical and Information Technology, Lund University, Lund, Sweden

ALG, 0000-0002-3229-5451

There has not been a satisfying numerical validation of the theory of effective waves in random particulate materials. Validation has been challenging because the theoretical methods for effective waves have been limited to random particulate media in infinite slabs or half-spaces, which require a very large number of particles to perform accurate numerical simulations. This paper offers a solution by providing, from first principles, a method to calculate effective waves for a sphere filled with particles for a spherically symmetric incident wave. We show that this case can excite exactly the same effective wavenumbers, which are the most important feature to validate for effective waves. To check correctness, we also deduce an integral equation method which does not assume the effective wave solution. Our methods are, in principal, valid for any frequency, particle volume fraction and disordered pair-correlation. With the methods we provide, it is now possible to validate, with a heavier Monte Carlo simulation, the predictions from effective wave theory.

1. Introduction

A particulate material is any material filled with an arrangement of small particles in a homogeneous

background medium, often with a disordered distribution. Typically, the particles are modelled by spheroids or ellipsoids. Examples of particulate materials include powders, slurries, emulsions, certain types of porous materials (where the pores are the particles) and particulate composites. These materials are common in industry, especially as precursor materials [1]. The development of accurate and efficient mathematical models is a prerequisite for using waves, such as sound and light, to measure these materials.

To get consistent predictions, and measurements, we need to model the average scattered wave, and not just waves scattered from one configuration of particles. In practice, this average is often achieved by averaging measurements over time or space. Without taking the average, our predictions and measurements would depend on the exact configuration of particles, which is often impossible to know. This average is assumed to be equivalent to an ensemble average over particle positions and properties, which means the particle statistics is ergodic [2]. There is a long history of developing theoretical frameworks to describe the average scattered wave, as well as the average intensity, for a random set of particles [3]. These theoretical methods have been adapted to electromagnetics and optics [2,4–7], and acoustics [8–10].

Plates filled with particles. So far attempts to numerically validate the theoretical methods have focused on plates and half-spaces filled with particles. This is likely because these were the cases which were best understood, from a theoretical standpoint. However, validating these scenarios requires the simulation of waves scattering within an infinite number of particles [11,12], or use of finite but very large numbers of particles as an approximation. Techniques from signal processing can be applied [13], but these are still computationally expensive. Accordingly, we are not aware of rigorous numerical validations of any of the average scattering theoretical methods that cover a wide range of frequencies and particle volume fractions.

Spherical symmetry. A clear way to overcome the numerical challenges is to validate models in which the particles occupy a bounded region, and therefore are finite in number. In this work, we focus on a sphere filled with particles (figure 1), and specialize to spherical symmetry, as this both simplifies the theoretical methods (that need validating), and will make any Monte Carlo validation far simpler, which will be the subject of a future numerical paper. We also demonstrate how validating this case serves to validate the effective dispersion equation of all cases. We note that there has been previous work focused on spheres filled with particles, which matched Monte Carlo simulations for very low volume fraction [14].

Statistical assumptions. All theoretical methods that apply beyond the low-frequency limit need to make statistical assumptions, with the two most common being: (i) a particular particle pair-correlation and (ii) a closure assumption, which is usually the Quasi-Crystalline Approximation (QCA), see [15] for some details. The first for the particle pair-correlation can be verified numerically without great difficultly [6]. The closure assumption, such as QCA, is very difficult to numerically validate, and to our knowledge there has been no clear numerical validation. By developing mathematical models that require a finite number of particles, and spherical symmetry, we pave the way for a broad validation of QCA and other statistical assumptions. Proving these models from first principles is the main goal of this paper.

Two mathematical methods. The main purpose of this paper is to provide two different mathematical methods for the average waves scattered from a particulate material in the shape of a sphere. Both methods are deduced from first principles to make clear exactly what assumptions are used. The first method, called the *integral method*, only assumes QCA. The second method, called the *effective wave method*, assumes both QCA and uses the effective wave assumption. By providing these two methods, for spherical symmetry, it will be possible in future work to validate the statistical assumptions by comparing with simulations of deterministic scattering algorithms [16]. Both methods are specialized to spherical symmetry, as this leads to significant simplifications, with the integral method being reduced to one dimension in space. Further, comparing the integral method with the effective waves methods serves as a way to validate the effective waves assumption, but note that there are proofs of the effective wave assumptions for plane waves [17]. We present two such comparisons in this paper, just as a demonstration that the equations are correct.

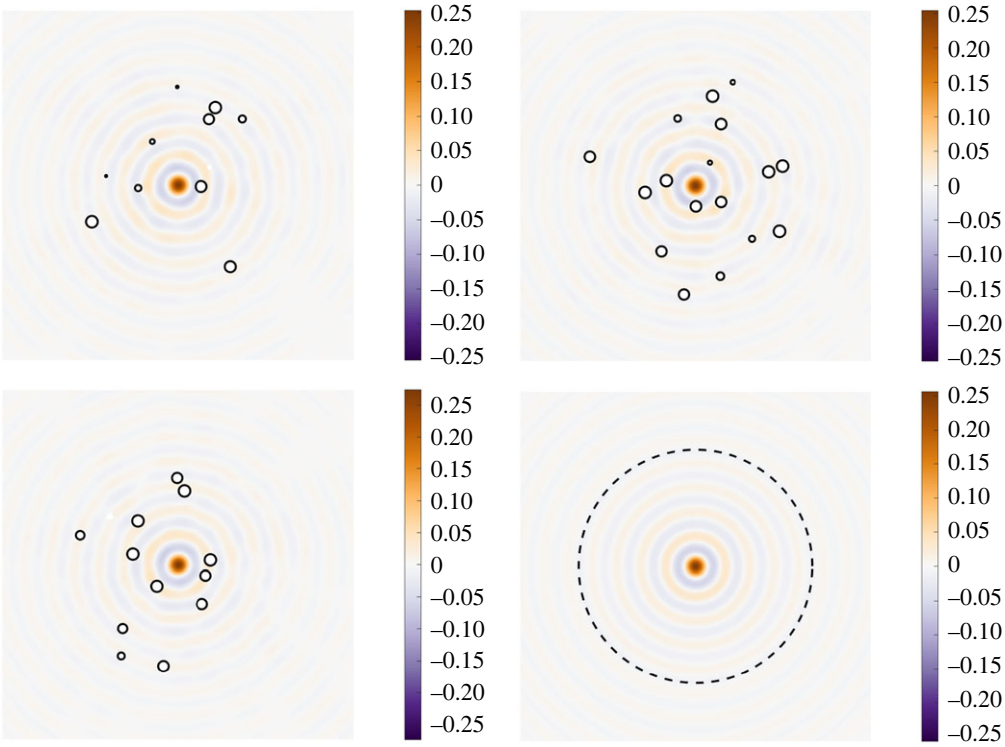

Figure 1. The top two and the bottom left images show the total field (Re u) in the plane $y = 0$ (spherically symmetric incident wave) for three random configurations of 160 particles confined within a large sphere $\mathcal{R}$ with radius $R = 20a$ (particle volume fraction 2%). Particle intersections with the plane $y = 0$ are plotted using solid lines. The bottom right image shows the average total field (Re $\langle u \rangle$) computed using Monte Carlo simulation with 250 random configurations. The aim of this paper is develop theoretical methods to calculate the bottom right image.

Effective wavenumbers. At the core of the effective waves method is the effective wavenumber $k_\star$. It is the parameter which depends on the particulate properties. One of the key contributions of this paper is that we show that spherically symmetry has the same effective wavenumbers as a plate filled with particles. Gower & Kristensson have shown [9] that the dispersion equation for a plate filled with particles is also the same as the dispersion equation for any geometry. Thus by numerically validating the case of spherical symmetry, we are in turn validating the dispersion equation for average waves in particulate materials in any geometry and with any source.

Testing exotic behaviour. Beyond just developing a method which can be easily validated numerically, the methods we develop here can also be used to test any disordered pair correlations and types of particles. Pair-correlations can have a dramatic effect, such as forming localized states [18], bandgaps [19] or lead to transparency [20]. Whereas different types of particles, such as resonators [21,22] or mixing multi-species [15], can also lead to strong scattering.

Both pair-correlations, and different types of particles, can be studied through theoretical methods that calculate the ensemble average. The methods we present capture all these effects and can quickly be evaluated to explore the parameter space, or verify exotic behaviour. For example, the effective wavenumbers dictate whether there is a bandgap or a window of transparency. That is, effective wavenumbers dictate when waves propagate or do not. Ultimately, it is worth numerically validating any exotic effect, by comparing with deterministic scattering which can now be easily achieved given the methods presented in this paper.

This paper. In §2, we explain how we account for scattering from one configuration of particles, with particles of a finite size. We then present the integral equation governing the average of wave scattering over all particle configurations, and introduce the main statistical assumptions.

In §3, we present, in a condensed self-contained form, the equations needed to solve the full integral equation with spherical symmetry in §3a, and the equations needed to solve the effective wave approximation for the same scenario in §3b.

In §4, we give some numerical results of both the methods, integral and effective wave, just to confirm correctness for broad frequency ranges. The software[1] for both methods is available at [23]. We also show results for an exotic pair-correlation: a form of hyperuniform disorder. The rest of the paper serves to formally derive the methods and check correctness.

In §5, we derive how to use spherical symmetry to reduce the fields that appear in the overall governing equation. In §§6 and 7, we apply the result of spherical symmetry to deduce the integral and effective wave method, respectively. In §8, we summarize some results of the paper and indicate future directions.

2. The average governing equations

(a) A collection of particles

We begin with a brief introduction to the deterministic many-particle scattering problem. We refer to [8,9,24] for the full details and references.

Consider J particles, where the ith particle is centred at the location $\boldsymbol{r}_i$.[2] For simplicity, we assume that all particles are identical and have radius a, although our results apply to multi-species or polydisperse materials with only minor adjustments. We will remark on the adjustments needed for our key results. The particles are located in a homogeneous, isotropic media with wavenumber k, which is either a real number or a complex number with a positive imaginary part.

We consider that scalar waves $u(\boldsymbol{r})$ can propagate in homogeneous media which satisfy the wave equation

$$\nabla^2 u(\boldsymbol{r}) + k^2 u(\boldsymbol{r}) = 0.$$

One such example would be acoustic waves, where $u(\boldsymbol{r})$ is the pressure. Specifying which type of scalar wave depends on the boundary conditions used for each particle, which in term is specified through the T-matrix given below.

We make use of scalar spherical waves:

$$\left.\begin{aligned} \mathrm{u}_n(k\boldsymbol{r}) &= \mathrm{h}_\ell^{(1)}(kr)\mathrm{Y}_n(\hat{\boldsymbol{r}}), \quad \text{(outgoing spherical waves)} \\ \text{and} \qquad \mathrm{v}_n(k\boldsymbol{r}) &= \mathrm{j}_\ell(kr)\mathrm{Y}_n(\hat{\boldsymbol{r}}), \quad \text{(regular spherical waves)} \end{aligned}\right\} \tag{2.1}$$

where $r = |\boldsymbol{r}|$, and n denotes a multi index $n = (\ell, m)$, with $\ell = 0, 1, 2, 3\ldots$ and $m = -\ell, -\ell+1, \ldots, -1, 0, 1, \ldots, \ell$. Here $\mathrm{h}_\ell^{(1)}(z)$ and $\mathrm{j}_\ell(z)$ denote the spherical Hankel and Bessel functions, respectively, and Y_n are the spherical harmonic basis functions that are orthonormal with respect to the standard inner product on the unit sphere [25]. See [9] for the definition of spherical harmonics we use, together with the main properties.

For a source located outside of all particles, we can write the total field $u(\boldsymbol{r})$ as a sum of the incident wave $u_{\mathrm{in}}(\boldsymbol{r})$ and all scattered waves in the form [26]

$$u(\boldsymbol{r}) = u_{\mathrm{in}}(\boldsymbol{r}) + u_{\mathrm{sc}}(\boldsymbol{r}), \quad u_{\mathrm{sc}}(\boldsymbol{r}) = \sum_{i=1}^{J} \sum_{n} f_n^i \mathrm{u}_n(k\boldsymbol{r} - k\boldsymbol{r}_i), \tag{2.2}$$

where we assumed $|\boldsymbol{r} - \boldsymbol{r}_i| > a$ for $i = 1, 2, \ldots, J$. The f_n^i will be determined by applying the boundary conditions on all particles. The field $\sum_n f_n^i \mathrm{u}_n(k\boldsymbol{r} - k\boldsymbol{r}_i)$ is the wave scattered from particle-i, and $n = (\ell, m)$ is implicitly summed over all admissible values.

[1] With examples given in https://juliawavescattering.github.io/EffectiveWaves.jl/dev/manual/sphere/.

[2] Throughout this paper, vector-valued quantities are denoted in italic boldface and vectors of unit length have a 'hat' or caret (^) over the symbol.

Typically, we assume the source that generated the incident wave u_{in} is outside of the material, given by the region $\mathcal{R}$. Let the centre of the sphere $\mathcal{R}$ be the origin of $\boldsymbol{r}$, then the regularity of incident wave implies that $u_{\text{in}}(\boldsymbol{r})$ for $\boldsymbol{r} \in \mathcal{R}$ is a smooth field, and therefore can be expanded in terms of regular spherical waves in the form:

$$u_{\text{in}}(\boldsymbol{r}) = \sum A_n \mathrm{v}_n(k\boldsymbol{r}),$$

as there cannot be any singularity of $u_{\text{in}}(\boldsymbol{r})$ for $\boldsymbol{r}$ close to the origin, the above cannot contain any outgoing waves of the form u_n.

As our aim is to have spherical symmetry (after ensemble averaging), to achieve this we keep only the spherically symmetric term in the expansion for the incident wave:

$$u_{\text{in}}(\boldsymbol{r}) = A_{\text{in}} \mathrm{v}_0(k\boldsymbol{r}), \quad \text{(spherically symmetric incident wave)}, \tag{2.3}$$

where A_{in} is the amplitude of the incident wave.

By applying the boundary conditions to every particle, or using a T-matrix, we can form a linear system to solve for the f_n^i [8,9,24,26]. This equation can be solved directly, but the computational cost is high for a large number of particles[3].

For methods that aim to characterize the particles, the computational cost becomes acute because the average field is needed, which requires repeated simulations. Using methods that directly compute the average field greatly reduces the computational cost.

To describe the response of each particle, and its boundary conditions, we use the T-matrix, and consider that all particles are identical, so they all share the same T-matrix. For example, for acoustics and a homogeneous spherical particle the T-matrix is diagonal with diagonal entries [8]:

$$T_{(\ell,m),(\ell,m)} = -\frac{\gamma \mathrm{j}_\ell'(ka)\mathrm{j}_\ell(k_o a) - \mathrm{j}_\ell(ka)\mathrm{j}_\ell'(k_o a)}{\gamma \mathrm{h}_\ell^{(1)\prime}(ka)\mathrm{j}_\ell(k_o a) - \mathrm{h}_\ell^{(1)}(ka)\mathrm{j}_\ell'(k_o a)} =: T_{(\ell,m)}, \tag{2.4}$$

where $\gamma = \rho_o k/(\rho k_o)$, a is the particle radius, ρ is the background density, while ρ_o and k_o are the density and wavenumber of the particle.

We note that for spherically symmetric particles, or for the average T-matrix of a particle that has been averaged over all orientations, we have that $T_{(\ell,m)} = T_{(\ell,0)}$ for every m [9,31,32]. As a shorthand, we define $T_\ell := T_{(\ell,0)}$. For the methods in this paper, we require that $T_{(\ell,m)} = T_{(\ell,0)}$.

(b) Ensemble average

Consider the case in which all particles are confined within a large sphere $\mathcal{R}$ with radius R, which is centred at the origin (figure 2). When ensemble averaging, we fix the particle volume fraction, and average over all possible particle positions. The centre $\boldsymbol{r}_j$ of the jth particle is confined within a sphere $\mathcal{R}_a$ with radius $R - a$. This guarantees that the whole particle is confined within $\mathcal{R}$.

The governing equation for the ensemble average of f_n^i, with no approximation, is [9]

$$\begin{aligned}\langle f_n\rangle(\boldsymbol{r}_1) &= T_\ell A_{\text{in}} \mathcal{V}_{(0,0)n}(k\boldsymbol{r}_1) \\ &\quad + T_\ell \sum_{n'} \int_{\mathcal{R}_a} \mathcal{U}_{n'n}(k\boldsymbol{r}_1 - k\boldsymbol{r}_2)\langle f_{n'}\rangle(\boldsymbol{r}_2, \boldsymbol{r}_1) g(\boldsymbol{r}_1, \boldsymbol{r}_2)\mathrm{n}(\boldsymbol{r}_2)\,\mathrm{d}\boldsymbol{r}_2,\end{aligned} \tag{2.5}$$

for all $\boldsymbol{r}_1 \in \mathcal{R}_a$ and admissible n, where we used (2.3), and the $\mathcal{U}_{nn'}$ and $\mathcal{V}_{nn'}$ are translation matrices of the spherical waves u_n and v_n, respectively (see appendix A). In the above, we used the notation

$$\langle f_n\rangle(\boldsymbol{r}_1) := \langle f_n^1\rangle(\boldsymbol{r}_1) \quad \text{and} \quad \langle f_n\rangle(\boldsymbol{r}_2, \boldsymbol{r}_2) := \langle f_n^2\rangle(\boldsymbol{r}_2, \boldsymbol{r}_1),$$

where the function $\langle f_{n'}\rangle(\boldsymbol{r}_1)$ is the ensemble average of $f_{n'}^1$ over all particle positions, while holding $\boldsymbol{r}_1$ fixed, while $\langle f_{n'}\rangle(\boldsymbol{r}_2, \boldsymbol{r}_1)$ is the ensemble average of $f_{n'}^2$ while holding $\boldsymbol{r}_1$ and $\boldsymbol{r}_2$ fixed. See [9] for

[3]Nevertheless, there are several software packages making substantial progress, e.g. MSTM (Multiple Sphere T-Matrix) [27,28] and other related approaches [29,30].

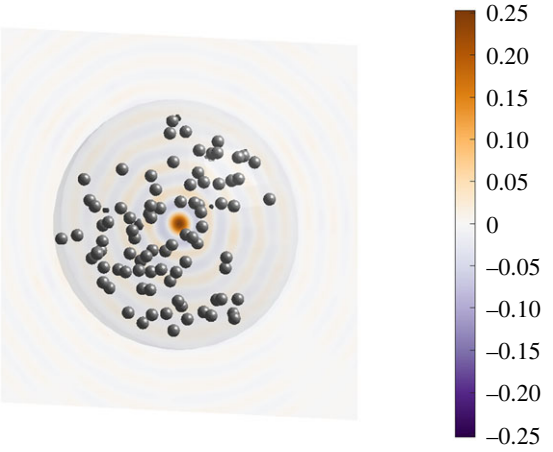

Figure 2. Visualization of a configuration of 160 particles confined within a large sphere $\mathcal{R}$ with radius $R = 20a$ (particle volume fraction 2%) and the corresponding total field (Re u).

details. We also introduced the particle number density $\mathfrak{n}(\boldsymbol{r}_2) = Jp(\boldsymbol{r}_2)$ and the pair correlation

$$g(\boldsymbol{r}_1, \boldsymbol{r}_2) = \frac{p(\boldsymbol{r}_1, \boldsymbol{r}_2)}{p(\boldsymbol{r}_1)p(\boldsymbol{r}_2)} \frac{J-1}{J}.$$

Here $p(\boldsymbol{r}_1)$ is the probability density of finding particle 1 in a volume element $\mathrm{d}\boldsymbol{r}_1$ centred at $\boldsymbol{r}_1$, while $p(\boldsymbol{r}_1, \boldsymbol{r}_2)$ is the probability density of finding particle 1 in a volume element $\mathrm{d}\boldsymbol{r}_1$ centred at $\boldsymbol{r}_1$ and particle 2 in a volume element $\mathrm{d}\boldsymbol{r}_2$ centred at $\boldsymbol{r}_2$.

The governing system (2.5) assumes a diagonal T-matrix associated with a spherical particle, or particles that are equally likely to be oriented in any direction. For details on non-spherical and polydisperse particles, see [9].

The ensemble average scattered field is then given by

$$\langle u_{\mathrm{sc}}(\boldsymbol{r})\rangle = \sum_n \int_{\mathcal{R}_a} \langle f_n\rangle(\boldsymbol{r}_1)\mathrm{u}_n(k\boldsymbol{r} - k\boldsymbol{r}_1)\mathfrak{n}(\boldsymbol{r}_1)\,\mathrm{d}\boldsymbol{r}_1. \tag{2.6}$$

Statistical assumptions. To use equation (2.5) to determine $\langle f_n\rangle(\boldsymbol{r}_1)$ we need to know the pair correlation $g(\boldsymbol{r}_1, \boldsymbol{r}_2)$ and the conditional average field $\langle f_{n'}\rangle(\boldsymbol{r}_2, \boldsymbol{r}_1)$. The most common approach for the conditional field is to approximate $\langle f_{n'}\rangle(\boldsymbol{r}_2, \boldsymbol{r}_1)$ by its conditional average in $\boldsymbol{r}_1$, the so-called *Quasi-Crystalline Approximation* (QCA):

$$\langle f_{n'}\rangle(\boldsymbol{r}_2, \boldsymbol{r}_1) \approx \langle f_{n'}\rangle(\boldsymbol{r}_2). \tag{2.7}$$

We refer to [15] for a brief discussion on the topic.

When choosing the pair-correlation $g(\boldsymbol{r}_1, \boldsymbol{r}_2)$ there are some restrictions: the particles are only distinguished by their position, so that $g(\boldsymbol{r}_2; \boldsymbol{r}_1) = g(\boldsymbol{r}_1; \boldsymbol{r}_2)$, and as p is a probability density, we have that

$$\int_{\mathcal{R}_a} p(\boldsymbol{r}_2)\,\mathrm{d}\boldsymbol{r}_2 = 1 \quad \text{and} \quad \int_{\mathcal{R}_a} g(\boldsymbol{r}_1; \boldsymbol{r}_2)p(\boldsymbol{r}_2)\,\mathrm{d}\boldsymbol{r}_2 = 1. \tag{2.8}$$

A common approximation, which is very accurate when $\boldsymbol{r}_1$ is away from the boundary of $\mathcal{R}_a$, is that $p(\boldsymbol{r}_i)$ is approximately a constant, which combined with (2.8) gives

$$p(\boldsymbol{r}_1) = \frac{1}{|\mathcal{R}_a|} = \frac{3}{4\pi(R-a)^3}, \quad \text{for } \boldsymbol{r}_1 \in \mathcal{R}_a, \tag{2.9}$$

where $|\mathcal{R}_a|$ is the volume of $\mathcal{R}_a$.

There are two essential properties for the pair-correlation for disordered particle positions:

$$g(\boldsymbol{r}_2, \boldsymbol{r}_1) = 0 \quad \text{for } |\boldsymbol{r}_1 - \boldsymbol{r}_2| < a_{12} \tag{2.10}$$

and

$$g(\boldsymbol{r}_2, \boldsymbol{r}_1) = 1 \quad \text{for } |\boldsymbol{r}_1 - \boldsymbol{r}_2| > b_{12}, \tag{2.11}$$

where a_{12} is the minimum allowed distance between the particle centres $\boldsymbol{r}_1$ and $\boldsymbol{r}_2$, and when the distance between any two particle centres is greater than b_{12}, then those particles become uncorrelated. See [4] for a review on correlated disordered media. We give examples of pair-correlations in §4 which shows numerical results.

Paper goal. The focus of this paper is to reduce (2.5) by using spherical symmetry. The result will be a one-dimensional integral equation, called the *Integral method*, and a semi-analytic approach called the *Effective wave method*. To solve the resulting equations, we still need to make use of QCA (2.7). Nevertheless, the simplified governing equation we deduce makes it simpler to study the effects and accuracy of QCA.

3. The spherically symmetric governing equations

Numerically solving (2.5) even for $n = (\ell, m)$ with $\ell = 0, \ldots, 5$ can be prohibitively expensive in three dimensions. We will use spherical symmetry to render the solution of (2.5) tractable. This is particularly important when, as arises in many applications, the goal is to solve for a wide range of frequencies, and for multi-species particles. See [9] for equations related to multi-species particulates.

In this section, we give all the main results of this paper, which can be used to solve for $\langle f_n \rangle(\boldsymbol{r}_1)$, which in turn can be used to get the average scattered field (2.6). All the proofs necessary to obtain these results are given in §§5–7.

Let (r_1, θ_1, ϕ_1) be the radial distance, polar angle, and azimuthal angle of $\boldsymbol{r}_1$. From spherical symmetry and the governing equation (2.5), we prove the reduced representations

$$g(\boldsymbol{r}_1, \boldsymbol{r}_2) = \sum_{\ell_1} \frac{2\ell_1 + 1}{4\pi} g_{\ell_1}(r_1, r_2) P_{\ell_1}(\hat{\boldsymbol{r}}_1 \cdot \hat{\boldsymbol{r}}_2), \tag{3.1}$$

$$\langle f_{(\ell,m)} \rangle(\boldsymbol{r}_1) = F_\ell(r_1) \mathrm{Y}^*_{(\ell,m)}(\theta_1, \phi_1) \tag{3.2}$$

and

$$\langle f_{(\ell,m)} \rangle(\boldsymbol{r}_2, \boldsymbol{r}_1) = \sum_{n_2 n_3} \frac{c_{(\ell,m)n_2 n_3}}{c_{(\ell,0)(\ell_2,0)(\ell_3,0)}} F_{\ell\ell_2\ell_3}(r_2, r_1) \mathrm{Y}^*_{n_2}(\theta_2, \phi_2) \mathrm{Y}^*_{n_3}(\theta_1, \phi_1), \tag{3.3}$$

where $n_2 = (\ell_2, m_2)$, $n_3 = (\ell_3, m_3)$, $\hat{\boldsymbol{r}}_1 = \boldsymbol{r}_1/|\boldsymbol{r}_1|$, the star $\circ^*$ denotes the conjugate of $\circ$, and the $c_{nn_2n_3} = c_{(\ell,m)n_2n_3}$ are real numbers which can be expressed in terms of the Wigner 3j symbols (A 7).

(a) The integral method

In §6, we show that substituting the representations above into (2.5), together with (2.7), (2.10) and (2.11), leads to the following governing equation for the function $F_\ell(r_1)$:

$$\boxed{F_\ell(r_1) = \sqrt{4\pi} T_\ell A_{\mathrm{in}} \mathrm{j}_\ell(kr_1)(-1)^\ell + T_\ell \sum_{\ell_2} \int_0^{R-a} C_{\ell\ell_2}(r_1, r_2) F_{\ell_2}(r_2)\, \mathrm{d}r_2,} \tag{3.4}$$

where

$$C_{\ell\ell_2}(r_1, r_2) := r_2^2 \mathfrak{n}(r_2) \chi_{\ell\ell_2}(r_1, r_2) 4\pi (-1)^\ell (2\ell_2 + 1), \tag{3.5}$$

for $|r_1 - r_2| > b_{12}$, and

$$C_{\ell\ell_2}(r_1, r_2) := r_2^2 \mathfrak{n}(r_2) \sum_{n_1=(\ell_1,m_1)} \sum_{\ell_4\ell_5\ell_6 m_2} \chi_{\ell_5\ell_6}(r_1, r_2) g_{\ell_1}(r_1, r_2) \frac{(-1)^{\ell_4} \mathrm{i}^{\ell-\ell_5-\ell_6-\ell_2}}{(4\pi)^2}$$
$$\times\, c_{(\ell,0)n_1(\ell_5,-m_1)} c_{n_1 n_2(\ell_6,m_1-m_2)} c_{(\ell,0)n_2(\ell_4,-m_2)} c_{(\ell_4,m_2)(\ell_5,m_1)(\ell_6,m_2-m_1)}, \tag{3.6}$$

for $|r_1 - r_2| \le b_{12}$. Here

$$\chi_{\ell_5\ell_6}(r_1, r_2) = (-1)^{\ell_6} \begin{cases} \mathrm{h}^{(1)}_{\ell_6}(kr_2)\mathrm{j}_{\ell_5}(kr_1) & \text{for } r_1 < r_2, \\ \mathrm{h}^{(1)}_{\ell_5}(kr_1)\mathrm{j}_{\ell_6}(kr_2) & \text{for } r_1 > r_2. \end{cases}$$

We can numerically solve (3.4) for $F_{\ell_1}(r_1)$ after choosing a pair-correlation $g(\boldsymbol{r}_1, \boldsymbol{r}_2)$, which determines the $g_{\ell_1}(r_1, r_2)$.

After numerically obtaining the field $F_\ell(r_1)$, we can then calculate the average scattered field (2.6) by substituting $\mathfrak{n}(\boldsymbol{r}_1) = \mathfrak{n}(r_1)$ due to isotropy, and using (3.2) to obtain

$$\langle u_{\mathrm{sc}}(\boldsymbol{r})\rangle = \mathfrak{F}\mathrm{u}_{(0,0)}(k\boldsymbol{r}), \tag{3.7}$$

where

$$\mathfrak{F} = \int_0^{R-a} \sum_\ell (-1)^\ell (2\ell+1) F_\ell(r_1)\mathrm{j}_\ell(kr_1) r_1^2 \mathfrak{n}(r_1)\,\mathrm{d}r_1. \tag{3.8}$$

The proof of this result is given in §6.

(b) The Effective wave method

An alternative formulation starts by using the representation

$$\langle f_n\rangle(\boldsymbol{r}_1) = \sum_{p=1} f_{p,n}(\boldsymbol{r}_1), \quad \text{where } \nabla^2 f_{p,n}(\boldsymbol{r}_1) + k_p^2 f_{p,n}(\boldsymbol{r}_1) = 0. \tag{3.9}$$

Here the wavenumbers k_p, known as the effective wavenumbers, need to be determined.

For most frequencies, volume fractions, and material parameters, only the $p = 1$ term in the representation is needed to obtain accurate results [17,33]. Specifically, frequencies and properties that lead to very strong scattering can trigger more than one effective wavenumber [34]. We also note that the other effective wavenumbers ($p > 1$) form a type of boundary layer, so if the radius of the material R is too small, the other effective wavenumbers could affect the transmitted field [17,34].

When we retain only the first $p = 1$ term in (3.9), the methods to solve for $\langle f_n\rangle(\boldsymbol{r}_1)$ are much simpler than numerically solving (3.4). In this paper, we demonstrate how to solve the spherically symmetric problem for just one effective wavenumber $k_\star = k_1$, so that

$$\nabla^2\langle f_n\rangle(\boldsymbol{r}_1) + k_\star^2\langle f_n\rangle(\boldsymbol{r}_1) = 0. \tag{3.10}$$

To further simplify the equations, we use:

$$g(\boldsymbol{r}_2, \boldsymbol{r}_1) = 1 + \delta g(\boldsymbol{r}_2, \boldsymbol{r}_1) \quad \text{for } a_{12} \le |\boldsymbol{r}_1 - \boldsymbol{r}_2| \le b_{12}, \tag{3.11}$$

and

$$\mathfrak{n}(r_1) = \mathfrak{n} \quad \text{(some constant)}, \tag{3.12}$$

where the second equation assumes that the particle number density is constant in space.

Details on the proofs in this section are provided in §7. The result of combining (3.10), (3.2), and [9, eqn (5.1)] leads to the representation

$$\boxed{\langle f_{(\ell,m)}\rangle(\boldsymbol{r}_1) = (-1)^m F_\ell v_{(\ell,-m)}(k_\star \boldsymbol{r}_1),} \quad \text{(the effective wave approximation)} \tag{3.13}$$

where F_ℓ and $k_\star$ remain to be determined.

Substituting the above form into [9, eqn (5.6)], which represents the general dispersion equation, we obtain a simpler dispersion equation:

$$\boxed{S_\ell + T_\ell \sum_{\ell'} G_{\ell\ell'} S_{\ell'} = 0,} \quad \text{(the eigensystem)}, \tag{3.14}$$

where $S_\ell = \mathrm{i}^{-\ell}\sqrt{2\ell+1}F_\ell$ and

$$G_{\ell\ell'} = \mathfrak{n} \sum_{\ell_3} c_{(\ell',0)(\ell,0)(\ell_3,0)} \mathrm{K}_{\ell_3} \mathrm{i}^{-\ell_3} \sqrt{4\pi(2\ell_3+1)}, \tag{3.15}$$

$$\mathrm{K}_{\ell_3} = a_{12} \frac{\mathrm{N}_{\ell_3}(ka_{12}, k_\star a_{12})}{k_\star^2 - k^2} - W_\ell, \tag{3.16}$$

$$\mathrm{N}_{\ell_3}(x,y) = x\mathrm{h}_\ell^{(1)\prime}(x)\mathrm{j}_\ell(y) - y\mathrm{h}_\ell^{(1)}(x)\mathrm{j}_\ell'(y) \tag{3.17}$$

and

$$W_\ell = \int_{a_{12}}^{b_{12}} \mathrm{h}_\ell(kr)\mathrm{j}_\ell(k_\star r)\delta g(r) r^2 \, \mathrm{d}r. \tag{3.18}$$

Equation (3.14) is exactly the same as the eigensystem for plane-waves with azimuthal symmetry given by [9, eqn (5.16)], which implies that the effective wavenumber $k_\star$ is the same. This means that the same wavenumbers, and the same statistical assumptions, for any geometry, can be tested here in the spherical symmetry case.

To calculate $k_\star$ we formulate a dispersion equation from (3.14) in the form

$$\boxed{\det \mathbf{M}(k_\star) = 0 \quad \text{where} \quad M_{\ell\ell'}(k_\star) = \delta_{\ell\ell'} + T_\ell G_{\ell\ell'}.} \quad \text{(the dispersion equation)} \tag{3.19}$$

Once we have calculated $k_\star$, we can calculate the direction of the vector F_ℓ by returning to (3.14) and solving for F_ℓ. To determine the amplitude of the vector F_ℓ we substitute the above form into [9, eqn (6.3)] to obtain an extra equation

$$\boxed{\sum_{\ell'} \frac{2\ell'+1}{(-1)^{\ell'}} \frac{R-a}{k^2 - k_\star^2} \mathrm{N}_{l'}(kR - ka, k_\star R - k_\star a) F_{\ell'} = \frac{A_{\text{in}}}{\sqrt{4\pi}}.} \quad \text{(boundary conditions)} \tag{3.20}$$

Finally, we can directly calculate the average scattered wave (2.6) by using [9, eqn (6.6)], followed by (3.13) and (A 5), which leads to the scattering coefficient

$$\mathfrak{F} = \sqrt{4\pi}\,\mathfrak{n} \frac{R-a}{k_\star^2 - k^2} \sum_\ell (2\ell+1)(-1)^\ell F_\ell M_\ell(k(R-a_1), k_\star(R-a_1)), \tag{3.21}$$

with $M_\ell(x,y) = x\mathrm{j}_\ell'(x)\mathrm{j}_\ell(y) - y\mathrm{j}_\ell(x)\mathrm{j}_\ell'(y)$. The average scattered wave is then given by

$$\boxed{\langle u_{\text{sc}}(\boldsymbol{r})\rangle = \mathfrak{F}\, \mathrm{u}_{(0,0)}(k\boldsymbol{r}), \quad \text{for } r > R.} \quad \text{(average scattered field)} \tag{3.22}$$

4. Numerical results

Here we show numerical results for both the Integral method, given in §3a, and the Effective wave method, given in §3b. The software[4] for both is available at [23].

The aim of this section is to show that both methods can use a variety of pair-correlations, and that the two methods match for many choices of parameters. Our goal is not to do an extensive exploration over the parameter space. The main conclusions of this section are:

— Changing the pair-correlation can have a dramatic affect on the average scattered wave. For example, by creating a lower frequency resonance. The methods of this paper let us

[4]With examples given in https://juliawavescattering.github.io/EffectiveWaves.jl/dev/manual/sphere/.

quickly and easily explore the properties of these exotic materials and any disordered pair-correlation.

— The Integral method, summarized in §3a, uses a Fourier series for the pair-correlation, which leads to an error called Gibbs phenomenon. It was found (see below) that this error had no effect on the results shown.

— The Effective wave method §3b is very close to the more intensive Integral method except in the regions where only one effective wavenumber is excited. This is fully expected as the only difference between the two methods is that the Integral method accounts for all the effective wavenumbers. See [17,33] for details on this.

We present the numerical results in terms of the far-field average scattered wave:

$$\langle u_\infty \rangle = \lim_{r\to\infty} r e^{-\mathrm{i}kr} \langle u_{\mathrm{sc}}(\boldsymbol{r})\rangle = -\frac{\mathrm{i}\mathfrak{F}}{\sqrt{4\pi}k}, \tag{4.1}$$

where $\mathfrak{F}$ is given by (3.8) for the integral method and by (3.21) for the effective wave method.

For this section we consider an acoustic wave, with wavespeed and mass density $c=\rho=1$. The radius of the containing sphere $\mathcal{R}$ is $R=5$, the radius of the particles $a=1.0$, and the T-matrix of each particle is given by (2.4). We consider two types of boundary conditions:

$$T_\ell = -\frac{\mathrm{j}_\ell(ka)}{\mathrm{h}^{(1)}_\ell(ka)}, \quad \text{(Dirichlet boundary conditions)} \tag{4.2}$$

and

$$T_\ell = -\frac{\mathrm{j}'_\ell(ka)}{\mathrm{h}^{(1)\prime}_\ell(ka)}. \quad \text{(Neumann boundary conditions)} \tag{4.3}$$

Isotropic pair-correlations. The first step is to choose a pair-correlation. For spherical particles, with isotropic distribution, in an infinite medium, the pair-correlation is a function of only the inter-particle distance[5]:

$$g(\boldsymbol{r}_1,\boldsymbol{r}_2) = g(|\boldsymbol{r}_1-\boldsymbol{r}_2|). \tag{4.4}$$

For finite materials the above is an approximation, but is often very accurate [6]. We will use the above for our numerical results below, but note that the methods developed in this paper apply to any pair-correlation that can be written as a function $g := g(r_1, r_2, \theta_{12})$, where θ_{12} is the angle between $\boldsymbol{r}_1$ and $\boldsymbol{r}_2$.

The pair-correlation's coefficients. To use the Integral method, we need to calculate the $g_{\ell_1}(r_1,r_2)$ that appear in (3.1). Note that the representation (3.1) is a type of Fourier series, as $\hat{\boldsymbol{r}}_1\cdot\hat{\boldsymbol{r}}_2 = \cos\theta_{12}$, and therefore $P_{\ell_1}(\cos\theta_{12})$ are trigonometric functions. As pair-correlation functions are discontinuous, this means that (3.1) can have significant errors near the discontinuities, i.e. Gibbs phenomenon.[6]

Hole-correction. Gibbs phenomenon is easy to see for the pair-correlation called hole-correction, which states that

$$g(|\boldsymbol{r}_1-\boldsymbol{r}_2|) = \begin{cases} 0 & |\boldsymbol{r}_1-\boldsymbol{r}_2| \le a_{12}, \\ 1 & |\boldsymbol{r}_1-\boldsymbol{r}_2| > a_{12}. \end{cases} \tag{4.5}$$

See figure 3 for an example of how particles can be distributed for hole-correction.

The result of using the representation (3.1) for hole-correction is shown in figure 4. Though as the pair-correlation only appears within integrals, the point-wise error shown in figure 4 is not a significant concern. In the results presented we increased the number of terms in the Fourier series until the results converged, which was typically around order $\ell_1 \le 20$, with ℓ_1 appearing in (3.1). Note that the Effective wave method accounts for the pair-correlation through the term (3.18) and does not need to represent the pair-correlation with a Fourier series.

[5]Excuse our abuse of notation where we use g to represent two different functions.

[6]See https://en.wikipedia.org/wiki/Gibbs_phenomenon for details.

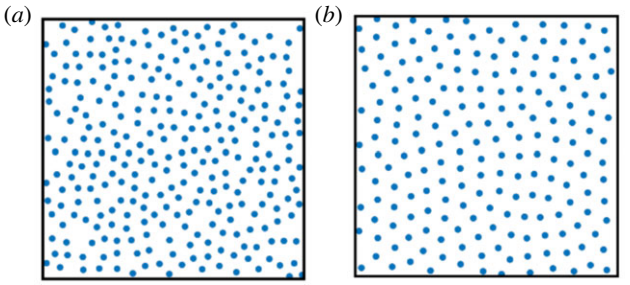

Figure 3. (*a*) An example of randomly distributed particles with only very short range correlation which is well approximated by Hole correction (4.5) or the Percus Yevick approximation [35]. (*b*) A distribution of particles that are locally periodic, with a random perturbation, and become uncorrelated as the inter-particle distance increases. This distribution is approximately given by a Hyperuniform disordered pair-correlation of the form figure 6. Adapted from Vynck *et al.* [4].

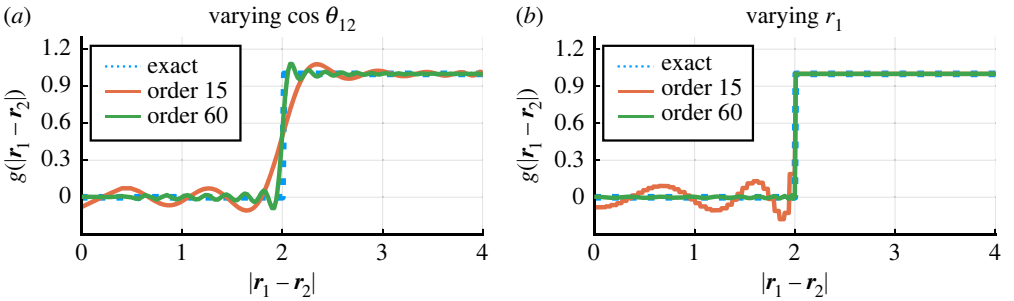

Figure 4. The two graphs compare the representation (3.1), when truncating the series, with the exact pair-correlation when using Hole-correction. The order refers to the maximum value for ℓ_1 used in (3.1). In both graphs, we fix $r_2 = 2$ and the particle radius $a = 1$. In (*a*), $r_1 = 2$ and we vary $\cos\theta_{12}$, and can clearly see Gibbs phenomenon near the discontinuity. In (*b*), we fix $\theta_{12} = 0$ and vary r_1.

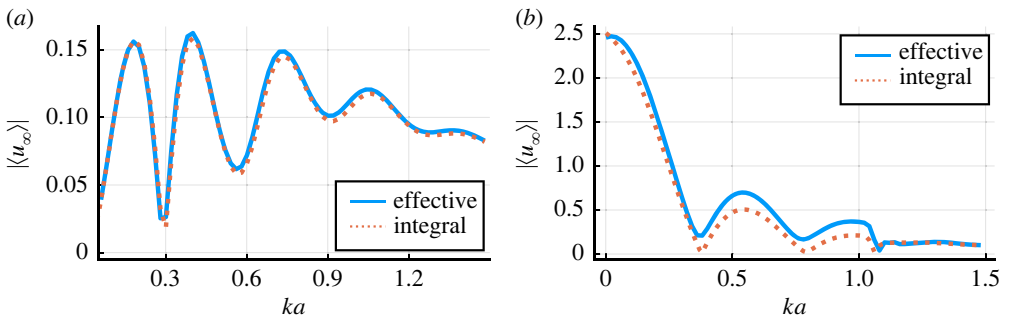

Figure 5. The figures show the far-field pattern for impenetrable Neumann (Dirichlet) particles on the *a* (*b*) with 15% volume fraction. The pair-correlation used is Hole-correction (4.5).

Figure 5 shows the far-field average scattered wave (4.1) of using the Hole-correction pair-correlation for both methods. Figure 5*a* uses impenetrable solid particles that have an infinite mass density, whereas (*b*) uses impenetrable void particles that have zero mass density. The results follow the same trends discussed in [33]: the particles with zero mass density excite more than just one effective wave, that is the sum in (3.9) needs to include more than just one term to more closely

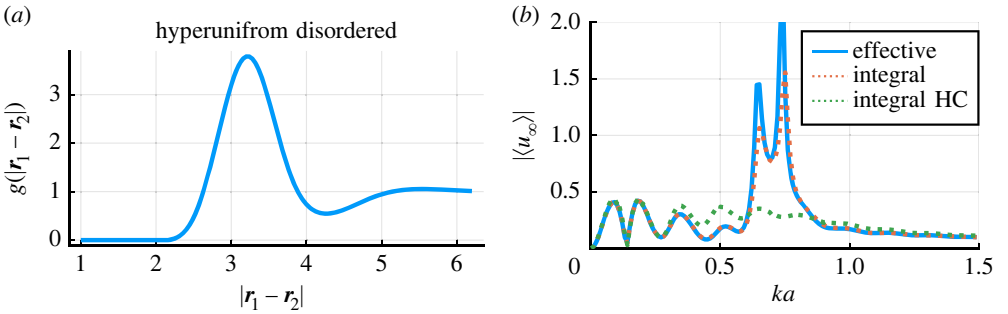

Figure 6. (*a*) We show one form of a Hyperuniform disordered pair-correlation: there is a preferred inter particle distance of about $|r_1 - r_2| \approx 3.3$, but particles become uncorrelated $|r_1 - r_2| > 6.0$. (*b*) The average far-field scattered wave for impenetrable Neumann particles with 20% volume fraction, where all lines use the Hyperuniform pair-correlation, except the dotted green line which uses the Hole-correlation pair-correlation.

match the Integral method (figure 5*b*) which accounts for all the terms in the sum in (3.9). On the other hand, as confirmed by figure 5*a*, a medium filled with sound hard particles tends to only excite the first effective wave $p = 1$, which is why the two methods match.

Hyperuniform disordered example. For an overview of different types of pair-correlations for disordered materials, see Vynck *et al.* [4]. For an example of how particles can be distributed for hyperuniform disordered materials, see figure 3.

To illustrate that our methods work for any choice of pair-correlation, we investigate one type of Hyperuniform disorder[7] with Neumann-type particles. For these types of materials the particles are strongly correlated to their neighbours, having a preferred inter-particle distance, but as the distance between any two particles increases they become uncorrelated. The example we use is shown in figure 6*a*, where we can see that particles prefer to be a distance of $|r_1 - r_2| = 3.3$ apart, but become uncorrelated around of $|r_1 - r_2| = 6.0$.

The result of using the Hyperuniform disordered pair-correlation is shown in figure 6*b*, which is also compared with the Integral method when using the Hole-correction (HC) pair correlation (4.5) (dotted green line). When compared with HC, the Hyperuniform material clearly exhibits a strong scattering between $0.6 < ka < 0.8$. This could indicate a resonance phenomenon with a large internal field, or could be like a bandgap with very little transmission. In the case of a bandgap very little of the incident wave is converted into a transmitted wave, so as a consequence, the incident wave is almost completely scattered [19]. To check whether the result shown in figure 6 is a bandgap, we turn to the dispersion diagram, which does not contain a stop band in this frequency range, which indicates that the result shown in figure 6 is a resonance of the whole region $\mathcal{R}$.

The discrepancy between the Integral and Effective wave method shown in the region $0.6 < ka < 0.8$ of figure 6 are again due to the Effective wave method only keeping the first term in the sum (3.9), whereas the Integral method includes all terms in the sum. It seems that in resonance more than one effective wave tends to be excited, but this requires further research to confirm.

5. Deducing spherical symmetry representations

The rest of this paper is dedicated to deducing the two methods: the Integral method in §3a and the Effective wave method in §3b. Some of the steps involved are challenging, so to help clarity we prove two theorems in this section whose results will be used many times in subsequent sections.

[7]In this work, we will not focus on which pair-correlations can be exactly realized by specific configurations of particles. This numerical section is just to demonstrate both the methods we developed.

The simplest symmetries to deduce, which are due to isotropy of the particle distribution, are those of the probability function and pair-correlation:

$$p(\boldsymbol{r}_1) = p(\mathbf{P}\boldsymbol{r}_1) \quad \text{and} \quad g(\boldsymbol{r}_1, \boldsymbol{r}_2) = g(\mathbf{P}\boldsymbol{r}_1, \mathbf{P}\boldsymbol{r}_2), \tag{5.1}$$

for any rotation matrix $\mathbf{P} \in \mathbb{R}^{3\times 3}$. Let (r_j, θ_j, ϕ_j) be the spherical coordinates of $\boldsymbol{r}_j$, where θ_j is the polar angle and ϕ_j is the azimuthal angle. The consequence of the first equation is that $p(\boldsymbol{r}_1) = p(r_1)$, that is, it does not depend on θ_1 or ϕ_1. Use of the second symmetry (5.1) to deduce the representation (3.1) is demonstrated in §a after the proof of the theorems below.

Proving symmetry reductions for the functions $\langle f_n \rangle$, shown in (3.2)–(3.3), is more complicated because the index n in $\langle f_n \rangle(\boldsymbol{r}_1)$, and $\langle f_n \rangle(\boldsymbol{r}_1, \boldsymbol{r}_1)$, depends on the orientation of the coordinate system. However, we will demonstrate that the symmetries for these fields can be written in a scalar form, which will allow us to use theorems 5.1 and 5.2.

The proofs below use the rotation formula for the spherical harmonics,

$$\mathrm{Y}_n(\mathbf{P}\hat{\boldsymbol{r}}_1) = \sum_{m'=-\ell}^{\ell} \mathrm{Y}_{(\ell,m')}(\hat{\boldsymbol{r}}_1)\mathrm{D}^{\ell}_{m'm}(\alpha, \beta, \gamma), \tag{5.2}$$

where $\mathbf{P}$ is any rotation matrix and where $D^{\ell}_{m'm}$ is the Wigner D-matrix [25, Section 4.1]. Here α, β and γ are the Euler angles corresponding to this rotation,[8] which are defined in [25, Section 1.3]. We often omit the Euler angles when they are the same for every appearance of the Wigner D-matrix.

Theorem 5.1.

Let $h(\cdot, \cdot)$ be a scalar-valued function that admits an expansion in spherical harmonics of the form

$$h(\hat{\boldsymbol{r}}_1, \hat{\boldsymbol{r}}_2) = \sum_{n_1 n_2} h_{n_1 n_2} \mathrm{Y}_{n_1}(\hat{\boldsymbol{r}}_1)\mathrm{Y}_{n_2}(\hat{\boldsymbol{r}}_2)$$

for any unit vectors $\hat{\boldsymbol{r}}_1, \hat{\boldsymbol{r}}_2$. If, for every rotation matrix $\mathbf{P}$, we have $h(\hat{\boldsymbol{r}}_1, \hat{\boldsymbol{r}}_2) = h(\mathbf{P}\hat{\boldsymbol{r}}_1, \mathbf{P}\hat{\boldsymbol{r}}_2)$ then

$$h_{(\ell_1,m_1)(\ell_2,m_2)} = \delta_{m_1,-m_2}\delta_{\ell_1,\ell_2}(-1)^{m_1} h_{(\ell_1,0)(\ell_1,0)}. \tag{5.3}$$

Proof. Using a spherical harmonic expansion, we have

$$h(\hat{\boldsymbol{r}}_1, \hat{\boldsymbol{r}}_2) = h(\mathbf{P}\hat{\boldsymbol{r}}_1, \mathbf{P}\hat{\boldsymbol{r}}_2) = \sum_{n_3 n_4} h_{n_3 n_4} \mathrm{Y}_{n_3}(\mathbf{P}\hat{\boldsymbol{r}}_1)\mathrm{Y}_{n_4}(\mathbf{P}\hat{\boldsymbol{r}}_2).$$

Using the rotation formula (5.2) yields

$$\sum_{n_3 n_4} h_{n_3 n_4} \mathrm{Y}_{n_3}(\hat{\boldsymbol{r}}_1)\mathrm{Y}_{n_4}(\hat{\boldsymbol{r}}_2) = \sum_{\substack{n_3=(\ell_3,m_3)\\ n_4=(\ell_4,m_4)}} h_{n_3 n_4} \cdot \sum_{m'_3 m'_4} \mathrm{Y}_{(\ell_3,m'_3)}(\hat{\boldsymbol{r}}_1)\mathrm{D}^{\ell_3}_{m'_3 m_3}\mathrm{Y}_{(\ell_4,m'_4)}(\hat{\boldsymbol{r}}_2)\mathrm{D}^{\ell_4}_{m'_4 m_4},$$

where the Euler angles of the Wigner D-matrix associated with $\mathbf{P}$ are implicit and we omit them for brevity.

Taking the inner products over the unit sphere with $Y_{n_1} = Y_{(\ell_1,m_1)}$ and $Y_{n_2} = Y_{(\ell_2,m_2)}$ with respect to $\hat{\boldsymbol{r}}_1$ and $\hat{\boldsymbol{r}}_2$, respectively, and using the orthogonality of the spherical harmonics, leads to

$$h_{n_1 n_2} = \sum_{m_3 m_4} h_{(\ell_1,m_3)(\ell_2,m_4)}\mathrm{D}^{\ell_1}_{m_1 m_3}\mathrm{D}^{\ell_2}_{m_2 m_4}. \tag{5.4}$$

Next, we integrate over all the Euler angles of the above Wigner-D matrices, and use (A 15) to obtain

$$h_{n_1 n_2} = \delta_{m_1,-m_2}\delta_{\ell_1,\ell_2}\frac{(-1)^{m_1}}{2\ell_1 + 1}\sum_{m_3} h_{(\ell_1,m_3)(\ell_1,-m_3)}(-1)^{m_3}. \tag{5.5}$$

[8] In [25, Section 1.3], the Euler angles are defined as rotations of the frame (passive rotations), and not of vectors. For example, if $\mathbf{P}$ rotates vectors around the z-axis such that $\phi \to \phi + \phi_0$, then this is equivalent to choosing $\alpha = -\phi_0$ and $\beta = \gamma = 0$. For this reason, some authors would use $\mathbf{P}^{-1}$ where we have used $\mathbf{P}$.

To rewrite the above in a more useful form, we take $m_2 = m_1 = 0$ and $\ell_2 = \ell_1$ to arrive at

$$h_{(\ell_1,0)(\ell_1,0)} = \frac{1}{2\ell_1+1}\sum_{m_3} h_{(\ell_1,m_3)(\ell_1,-m_3)}(-1)^{m_3},$$

which substituted in the right side of (5.5) leads to (5.3). To complete the proof, we see that (5.3) is the solution to (5.4), which can be shown by substituting the above into (5.4) and then using the property (A 14). ■

Theorem 5.2.

Let $h(\cdot,\cdot,\cdot)$ be a scalar-valued function that admits an expansion in spherical harmonics of the form

$$h(\hat{\mathbf{r}}_1,\hat{\mathbf{r}}_2,\hat{\mathbf{r}}_3) = \sum_{n_1n_2n_3} h_{n_1n_2n_3}\mathrm{Y}_{n_1}(\hat{\mathbf{r}}_1)\mathrm{Y}_{n_2}(\hat{\mathbf{r}}_2)\mathrm{Y}_{n_3}(\hat{\mathbf{r}}_3) \tag{5.6}$$

for any unit vectors $\hat{\mathbf{r}}_1,\hat{\mathbf{r}}_2,\hat{\mathbf{r}}_3$. Then $h(\hat{\mathbf{r}}_1,\hat{\mathbf{r}}_2,\hat{\mathbf{r}}_3) = h(\mathbf{P}\hat{\mathbf{r}}_1,\mathbf{P}\hat{\mathbf{r}}_2,\mathbf{P}\hat{\mathbf{r}}_3)$ for every rotation matrix $\mathbf{P}$ holds if and only if

$$\begin{cases} h_{n_1n_2n_3} = 0, & \text{when } \{\ell_1\ell_2\ell_3\} = 0, \\ h_{n_1n_2n_3}\begin{pmatrix}\ell_1 & \ell_2 & \ell_3\\ 0 & 0 & 0\end{pmatrix} = \begin{pmatrix}\ell_1 & \ell_2 & \ell_3\\ m_1 & m_2 & m_3\end{pmatrix} h_{(\ell_1,0)(\ell_2,0)(\ell_3,0)}, & \text{otherwise.}\end{cases} \tag{5.7}$$

Proof. First we start by defining the triangular delta

$$\{\ell_1\ell_2\ell_3\} = \begin{cases} 1 & \text{if } |\ell_1-\ell_2| \le \ell_3 \le |\ell_1+\ell_2|, \\ 0 & \text{else.}\end{cases}$$

An argument similar to that employed in the proof of theorem 5.1 leads to

$$h_{(\ell_1,m_1)(\ell_2,m_2)(\ell_3,m_3)} = \begin{pmatrix}\ell_1 & \ell_2 & \ell_3\\ m_1 & m_2 & m_3\end{pmatrix}\sum_{m_1'm_2'm_3'} h_{(\ell_1,m_1')(\ell_2,m_2')(\ell_3,m_3')}\begin{pmatrix}\ell_1 & \ell_2 & \ell_3\\ m_1' & m_2' & m_3'\end{pmatrix}. \tag{5.8}$$

Note that if $\{\ell_1\ell_2\ell_3\} = 0$, then both Wigner 3j symbols appearing above are zero and therefore $h_{n_1n_2n_3} = 0$. Now we suppose that $\{\ell_1\ell_2\ell_3\} \neq 0$, and choose $m_1 = m_2 = m_3 = 0$ to obtain

$$h_{(\ell_1,0)(\ell_2,0)(\ell_3,0)} = \begin{pmatrix}\ell_1 & \ell_2 & \ell_3\\ 0 & 0 & 0\end{pmatrix}\sum_{m_1'm_2'm_3'} h_{(\ell_1,m_1')(\ell_2,m_2')(\ell_3,m_3')}\begin{pmatrix}\ell_1 & \ell_2 & \ell_3\\ m_1' & m_2' & m_3'\end{pmatrix}. \tag{5.9}$$

Multiplying both sides by $\left(\begin{smallmatrix}\ell_1 & \ell_2 & \ell_3\\ m_1 & m_2 & m_3\end{smallmatrix}\right)$ gives

$$\begin{aligned} &h_{(\ell_1,0)(\ell_2,0)(\ell_3,0)}\begin{pmatrix}\ell_1 & \ell_2 & \ell_3\\ m_1 & m_2 & m_3\end{pmatrix} \\ &\quad= \begin{pmatrix}\ell_1 & \ell_2 & \ell_3\\ m_1 & m_2 & m_3\end{pmatrix}\begin{pmatrix}\ell_1 & \ell_2 & \ell_3\\ 0 & 0 & 0\end{pmatrix}\sum_{m_1'm_2'm_3'} h_{(\ell_1,m_1')(\ell_2,m_2')(\ell_3,m_3')}\begin{pmatrix}\ell_1 & \ell_2 & \ell_3\\ m_1' & m_2' & m_3'\end{pmatrix}. \end{aligned} \tag{5.10}$$

Multiplying (5.8) by $\left(\begin{smallmatrix}\ell_1 & \ell_2 & \ell_3\\ m_1 & m_2 & m_3\end{smallmatrix}\right)$ and substituting (5.10) into the right-hand side leads to (5.7).

To complete the proof, we show that using (5.7) leads to (5.8). By substituting (5.7) into the right side of (5.8), and using the orthogonality relation (A 10) we obtain the left side of (5.8). ■

(a) Spherical symmetry of the pair-correlation

We can now apply the theorem 5.1 to the pair correlation $g(\boldsymbol{r}_1,\boldsymbol{r}_2)$ defined in (5.1). Because g is a square integrable function in the angular variables with fixed r_1 and r_2, it admits the

representation

$$g(\boldsymbol{r}_1,\boldsymbol{r}_2)=\sum_{n_1n_2} g_{n_1n_2}(r_1,r_2)\mathrm{Y}_{n_1}(\hat{\boldsymbol{r}}_1)\mathrm{Y}_{n_2}(\hat{\boldsymbol{r}}_2).$$

For every fixed radial distances r_1 and r_2, we can apply theorem 5.1 to obtain $g_{n_1n_2}(r_1,r_2)=\delta_{m_1,-m_2}\delta_{\ell_1,\ell_2}(-1)^{m_1}g_{(\ell_1,0)(\ell_1,0)}(r_1,r_2)$. Substitute this into the representation above gives

$$g(\boldsymbol{r}_1,\boldsymbol{r}_2)=\sum_{\ell_1} g_{\ell_1}(r_1,r_2)\sum_{m_1=-\ell_1}^{\ell_1}\mathrm{Y}_{(\ell_1,m_1)}(\hat{\boldsymbol{r}}_1)\mathrm{Y}^*_{(\ell_1,m_1)}(\hat{\boldsymbol{r}}_2) \tag{5.11}$$

where we used $(-1)^{m_1}\mathrm{Y}_{(\ell_1,-m_1)}(\hat{\boldsymbol{r}}_2)=\mathrm{Y}^*_{n_1}(\hat{\boldsymbol{r}}_2)$ and defined $g_{\ell_1}:=g_{(\ell_1,0)(\ell_1,0)}$.

Using the addition theorem for the Legendre Polynomials [36, ch. 8] yields the alternative form (3.1), which is clearly invariant when applying the same rotation to $\hat{\boldsymbol{r}}_1$ and $\hat{\boldsymbol{r}}_2$.

(b) Spherical symmetry of f_n

It was shown in [9, Section 3.4] with an informal method how to deduce restrictions on the field $\langle f_n\rangle(\boldsymbol{r}_1)$ imposed by symmetries. The same informal method suggests the symmetries (5.14) and (5.15), and below we provide a rigorous proof.

Let us define, for univariate or bivariate functions h, the operation $\circ^{\mathbf{P}}$ in the form

$$h^{\mathbf{P}}_n(\boldsymbol{r}_1):=\sum_{m'=-\ell}^{\ell}\mathrm{D}^{\ell}_{mm'}h_{(\ell,m')}(\mathbf{P}\boldsymbol{r}_1) \tag{5.12}$$

and

$$h^{\mathbf{P}}_n(\boldsymbol{r}_2,\boldsymbol{r}_1):=\sum_{m'=-\ell}^{\ell}\mathrm{D}^{\ell}_{mm'}h_{(\ell,m')}(\mathbf{P}\boldsymbol{r}_2,\mathbf{P}\boldsymbol{r}_1). \tag{5.13}$$

Theorem 5.3.

Assume the governing equation (2.5) has a unique solution after making a closure approximation, such as the quasi-crystalline approximation (2.7), and that the material is statistically isotropic. Then

$$\langle f_n\rangle(\boldsymbol{r}_1)=\langle f^{\mathbf{P}}_n\rangle(\boldsymbol{r}_1) \tag{5.14}$$

and

$$\langle f_n\rangle(\boldsymbol{r}_2,\boldsymbol{r}_1)=\langle f^{\mathbf{P}}_n\rangle(\boldsymbol{r}_2,\boldsymbol{r}_1), \tag{5.15}$$

for every $\boldsymbol{r}_1$, $\boldsymbol{r}_2$, and all Euler angles α, β and γ of $\mathrm{D}^{\ell}_{mm'}$. Note we have made an abuse of notation such that $\langle f_n\rangle^{\mathbf{P}}=\langle f^{\mathbf{P}}_n\rangle$.

Proof. To start, the statistical isotropy of the particles implies that $p(\mathbf{P}\boldsymbol{r}_1)=p(\boldsymbol{r}_1)$ and $g(\mathbf{P}\boldsymbol{r}_1,\mathbf{P}\boldsymbol{r}_2)=g(\boldsymbol{r}_1,\boldsymbol{r}_2)$, for every rotation matrix $\mathbf{P}$ and points $\boldsymbol{r}_1$ and $\boldsymbol{r}_2$.

Let us use the following shorthand:

$$K_{n'n}[h](\boldsymbol{r}_1)=\int_{\mathcal{R}}\mathcal{U}_{n'n}(k\boldsymbol{r}_1-k\boldsymbol{r}_2)h(\boldsymbol{r}_2,\boldsymbol{r}_1)g(\boldsymbol{r}_1,\boldsymbol{r}_2)\mathrm{n}(\boldsymbol{r}_2)\,\mathrm{d}\boldsymbol{r}_2, \tag{5.16}$$

then the governing equation (2.5) becomes

$$\langle f_n\rangle(\boldsymbol{r}_1)=T_\ell A_{\mathrm{in}}\mathcal{V}_{(0,0)n}(k\boldsymbol{r}_1)+T_\ell\sum_{n'}K_{n'n}[\langle f_{n'}\rangle](\boldsymbol{r}_1). \tag{5.17}$$

We must show that

$$\langle f^{\mathbf{P}}_{(\ell,m)}\rangle(\boldsymbol{r}_1)=T_\ell A_{\mathrm{in}}\mathcal{V}_{(0,0)(\ell,m)}(k\boldsymbol{r}_1)+T_\ell\sum_{n'}K_{n'(\ell,m)}[\langle f^{\mathbf{P}}_{n'}\rangle](\boldsymbol{r}_1). \tag{5.18}$$

Equations (5.14) and (5.15) then follow as a consequence of uniqueness of $\langle f_n\rangle$.[9]

[9]The system (5.17) only has a solution when using a closure assumption such as (2.7). Our proof holds for any closure assumption that leads to unique solutions.

To show (5.18), we substitute $\boldsymbol{r}_1$ for $\mathbf{P}\boldsymbol{r}_1$ in (2.5), and multiply both sides by the rotation $D^{\ell}_{m''m}$ and sum over m to obtain

$$\langle f^{\mathbf{P}}_{(\ell,m'')}\rangle(\boldsymbol{r}_1) = T_\ell A_{\text{in}} \sum_{m=-\ell}^{\ell} \mathrm{D}^{\ell}_{m''m} \mathcal{V}_{(0,0)n}(k\mathbf{P}\boldsymbol{r}_1) + T_\ell \sum_{n'} \sum_{m=-\ell}^{\ell} \mathrm{D}^{\ell}_{m''m} K_{n'n}[\langle f_{n'}\rangle](\mathbf{P}\boldsymbol{r}_1). \tag{5.19}$$

The left side already matches the left side of (5.18). In appendix B, we show that the first term on the right side matches the corresponding term in (5.17), and in appendix C we show that the second term on the right side matches the corresponding term in (5.17), which completes the proof. ■

6. Deducing the integral equations

In this section, we use the symmetries (3.1) and (3.2) to reduce the governing system (2.5) to a one-dimensional integral equation that can be efficiently solved using numerical methods.

Substituting (2.7), (3.1) and (3.2) into system (2.5) leads to

$$F_\ell(r_1)\mathrm{Y}^*_{(\ell,m)}(\hat{\boldsymbol{r}}_1) = T_\ell A_{\text{in}} \mathcal{V}_{(0,0)(\ell,m)}(k\boldsymbol{r}_1) + T_\ell \sum_{n_2} K_{n_2(\ell,m)}[\langle f_{n_2}\rangle](\boldsymbol{r}_1), \tag{6.1}$$

where we can simplify

$$\begin{aligned}
&\sum_{(\ell_2,m_2)} K_{(\ell_2,m_2)n}[\langle f_{(\ell_2,m_2)}\rangle](\boldsymbol{r}_1)\\
&\quad= \sum_{(\ell_1,m_1)(\ell_2,m_2)} \mathrm{Y}^*_{n_1}(\hat{\boldsymbol{r}}_1) \int_{\mathcal{R}_a} \mathcal{U}_{(\ell_2,m_2)n}(k\boldsymbol{r}_1 - k\boldsymbol{r}_2)\mathrm{Y}_{(\ell_1,m_1)}(\hat{\boldsymbol{r}}_2)\\
&\qquad\times \mathrm{Y}^*_{(\ell_2,m_2)}(\hat{\boldsymbol{r}}_2)F_{\ell_2}(r_2)g_{\ell_1}(r_1,r_2)\mathfrak{n}(r_2)\,\mathrm{d}\boldsymbol{r}_2\\
&\quad= \sum_{\substack{(\ell_1,m_1)\\(\ell_2,m_2)}} \sum_{\substack{(\ell_4,m_4)\\(\ell_5,m_5)}} \sum_{(\ell_6,m_6)} \mathrm{Y}^*_{(\ell_1,m_1)}(\hat{\boldsymbol{r}}_1)\mathrm{Y}^*_{(\ell_5,m_5)}(\hat{\boldsymbol{r}}_1) \int_{\mathcal{R}_a} \mathrm{Y}_{(\ell_1,m_1)}(\hat{\boldsymbol{r}}_2)\mathrm{Y}^*_{(\ell_2,m_2)}(\hat{\boldsymbol{r}}_2)\mathrm{Y}^*_{(\ell_6,m_6)}(\hat{\boldsymbol{r}}_2)\\
&\qquad\times c_{(\ell_2,m_2)n(\ell_4,-m_4)}c_{(\ell_4,m_4)(\ell_5,m_5)(\ell_6,m_6)}(-1)^{m_4}\chi_{\ell_5\ell_6}(r_1,r_2)F_{\ell_2}(r_2)\\
&\qquad\times g_{\ell_1}(r_1,r_2)\mathfrak{n}(r_2)\,\mathrm{d}\boldsymbol{r}_2\\
&\quad= \sum_{\substack{(\ell_1,m_1)\\(\ell_2,m_2)}} \sum_{\substack{(\ell_4,m_4)\\(\ell_5,m_5)}} \sum_{(\ell_6,m_6)} \mathrm{Y}^*_{(\ell_1,m_1)}(\hat{\boldsymbol{r}}_1)\mathrm{Y}^*_{(\ell_5,m_5)}(\hat{\boldsymbol{r}}_1) \int_0^{R-a_2} r_2^2\,\mathrm{d}r_2 \mathrm{i}^{\ell_1-\ell_6-\ell_2}(4\pi)^{-1}\\
&\qquad\times (-1)^{m_4}c_{(\ell_1,m_1)(\ell_2,m_2)(\ell_6,m_6)}c_{(\ell_2,m_2)n(\ell_4,-m_4)}c_{(\ell_4,m_4)(\ell_5,m_5)(\ell_6,m_6)}\chi_{\ell_5\ell_6}(r_1,r_2)\\
&\qquad\times F_{\ell_2}(r_2)g_{\ell_1}(r_1,r_2)\mathfrak{n}(r_2),
\end{aligned} \tag{6.2}$$

where we used (2.7) and, in the penultimate line, used (A 1) and (A 3) to obtain

$$\begin{aligned}
\mathcal{U}_{n_2n}(k\boldsymbol{r}_1 - k\boldsymbol{r}_2) &= \sum_{n_4} c_{n_2nn_4}\mathrm{u}_{n_4}(k\boldsymbol{r}_1 - k\boldsymbol{r}_2)\\
&= \sum_{n_4(\ell_5,m_5)} c_{n_2n(\ell_4,m_4)}\Big[(-1)^{\ell_4+\ell_5}\chi_{r_1<r_2}\mathcal{U}_{(\ell_4,m_4)(\ell_5,m_5)}(k\boldsymbol{r}_2)\mathrm{v}_{(\ell_5,m_5)}(k\boldsymbol{r}_1)\\
&\quad + (-1)^{\ell_5}\chi_{r_1>r_2}\mathcal{U}_{(\ell_4,m_4)(\ell_5,m_5)}(k\boldsymbol{r}_1)\mathrm{v}_{(\ell_5,m_5)}(k\boldsymbol{r}_2)\Big]\\
&= \sum_{\substack{(\ell_4,m_4)(\ell_5,m_5)\\(\ell_6,m_6)}} c_{n_2n(\ell_4,m_4)}c_{(\ell_4,-m_4)(\ell_5,m_5)(\ell_6,m_6)}(-1)^{m_4}\mathrm{Y}^*_{(\ell_6,m_6)}(\hat{\boldsymbol{r}}_2)\mathrm{Y}^*_{(\ell_5,m_5)}(\hat{\boldsymbol{r}}_1)\chi_{\ell_5\ell_6}(r_1,r_2),
\end{aligned} \tag{6.3}$$

where we used the definition

$$\chi_{\ell_5\ell_6}(r_1,r_2)=\chi_{r_1<r_2}(-1)^{\ell_6}\mathrm{h}^{(1)}_{\ell_6}(kr_2)\mathrm{j}_{\ell_5}(kr_1)+\chi_{r_1>r_2}(-1)^{\ell_6}\mathrm{h}^{(1)}_{\ell_5}(kr_1)\mathrm{j}_{\ell_6}(kr_2),$$

and $\chi_{r_1>r_2}=1$ if $r_1>r_2$, otherwise it is zero.

To further simplify, we use (A 3) to write

$$\mathcal{V}_{(0,0)(\ell,m)}(k\boldsymbol{r}_1)=\sqrt{4\pi}A_{\mathrm{in}}(-1)^{\ell}\mathrm{j}_{\ell}(kr_1)\mathrm{Y}^{*}_{(\ell,m)}(\hat{\boldsymbol{r}}_1), \tag{6.4}$$

and then go back to (6.1), multiply both sides by $\mathrm{Y}_{n_0}(\hat{\boldsymbol{r}}_1)$, and integrate over $d\Omega_1$ to obtain

$$F_{\ell}(r_1)\delta_{n,n_0}=\sqrt{4\pi}T_{\ell}A_{\mathrm{in}}(-1)^{\ell}\mathrm{j}_{\ell}(kr_1)\delta_{n,n_0}+T_{\ell}\int\sum_{n'}K_{n'n}[\langle f_{n'}\rangle](\boldsymbol{r}_1)\mathrm{Y}_{n_0}(\hat{\boldsymbol{r}}_1)\,\mathrm{d}\Omega_1, \tag{6.5}$$

where, after using (A 4), we have

$$\begin{aligned}\int\sum_{n'}K_{n'n}[\langle f_{n'}\rangle](\boldsymbol{r}_1)\mathrm{Y}_{n_0}(\hat{\boldsymbol{r}}_1)\,\mathrm{d}\Omega_1=&\sum_{\substack{(\ell_1,m_1)\\(\ell_2,m_2)}}\sum_{\substack{(\ell_4,m_4)\\(\ell_5,m_5)}}\sum_{(\ell_6,m_6)}\int_0^{R-a_2}r_2^2\,\mathrm{i}^{\ell_0-\ell_5-\ell_6-\ell_2}(-1)^{m_4}(4\pi)^{-2}\\&\times c_{n_0n_1n_5}c_{n_1n_2n_6}c_{n_2n(\ell_4,-m_4)}c_{n_4n_5n_6}\\&\times\chi_{\ell_5\ell_6}(r_1,r_2)F_{\ell_2}(r_2)g_{\ell_1}(r_1,r_2)\mathfrak{n}(r_2)\,\mathrm{d}r_2,\end{aligned} \tag{6.6}$$

where we used the convention $n_j=(\ell_j,m_j)$ to save space.

Owing to symmetry, the above must simplify. In appendix F, we demonstrate this in detail to obtain (F 5), which leads to

$$\int\sum_{n'}K_{n'(l,m)}[\langle f_{n'}\rangle](\boldsymbol{r}_1)\mathrm{Y}_{n_0}(\hat{\boldsymbol{r}}_1)\,\mathrm{d}\Omega_1=\delta_{(l,m),n_0}\int\sum_{n'}K_{n'(\ell,0)}[\langle f_{n'}\rangle](\boldsymbol{r}_1)\mathrm{Y}_{(\ell,0)}(\hat{\boldsymbol{r}}_1)\,\mathrm{d}\Omega_1. \tag{6.7}$$

The proof of the above holds for any choice of $F_{\ell_2}(r_2)$ and $g_{\ell_1}(r_1,r_2)$. Owing to this, combining (6.6) and (6.7) suggests that

$$\begin{aligned}&\sum_{m_1m_2m_4m_5m_6}(-1)^{m_4}c_{n_0n_1n_5}c_{n_1n_2n_6}c_{n_2n(\ell_4,-m_4)}c_{n_4n_5n_6}\\&\quad=\delta_{n,n_0}\sum_{m_1m_2m_4m_5m_6}(-1)^{m_4}c_{(\ell,0)n_1n_5}c_{n_1n_2n_6}c_{n_2(\ell,0)(\ell_4,-m_4)}c_{n_4n_5n_6}\\&\quad=\delta_{n,n_0}\sum_{m_1m_2}(-1)^{m_2}c_{(\ell,0)n_1(\ell_5,-m_1)}c_{n_1n_2(\ell_6,m_1-m_2)}c_{n_2(\ell,0)(\ell_4,m_2)}c_{(\ell_4,m_2)(\ell_5,m_1)(\ell_6,m_2-m_1)}.\end{aligned} \tag{6.8}$$

The identity (6.8) does not seem to be a typical orthogonality result of Wigner 3j symbols so we have verified it numerically. Returning to (6.5), and using the above, we reach our governing integral equation (3.4).

Solving (3.4) can be made more efficient for random media by using (2.11), which leads to $g_{\ell_1}(r_1,r_2)=4\pi\delta_{\ell_1,0}$ for $|r_1-r_2|>b_{12}$, and as a consequence:

$$\begin{aligned}C_{\ell\ell_2}(r_1,r_2)=&\,r_2^2\mathfrak{n}(r_2)\chi_{\ell\ell_2}(r_1,r_2)g_0(r_1,r_2)\frac{1}{(4\pi)^2}\\&\times\sqrt{4\pi}\sum_{m_2}c_{(\ell_2,-m_2)(\ell_2,-m_2)(0,0)}(-1)^{\ell}\sum_{\ell_4m_4}c_{n_2n_4(\ell,0)}c_{n_2n_4(\ell,0)}\\=&\,r_2^2\mathfrak{n}(r_2)\chi_{\ell\ell_2}(r_1,r_2)4\pi(-1)^{\ell}(2\ell_2+1)\quad\text{for }|r_1-r_2|>b_{12}.\end{aligned} \tag{6.9}$$

7. Deducing the effective wave equations

Combining the assumption (3.10), we can perform an expansion of regular spherical waves:

$$\langle f_n\rangle(\boldsymbol{r}_1)=\sum_{n_1} F_{nn_1}\mathrm{v}_{n_1}(k_\star \boldsymbol{r}_1) \tag{7.1}$$

and

$$\langle f_n\rangle(\boldsymbol{r}_1,\boldsymbol{r}_2)=\sum_{n_1n_2} F'_{nn_1n_2}\mathrm{v}_{n_1}(k_\star \boldsymbol{r}_1)\mathrm{v}_{n_2}(k_\star \boldsymbol{r}_1), \tag{7.2}$$

where F_{nn_1} and $F'_{nn_1n_2}$ are independent of r_1. These expansions are known to converge when $\mathcal{R}$ is a sphere [9].

Substituting (3.11)–(3.12) into the governing equation (2.5), and using (2.7), we can split the integral on the right side into two parts:

$$\begin{aligned}\langle f_{(\ell,m)}\rangle(\boldsymbol{r}_1)=T_\ell \mathcal{V}_{(0,0)(\ell,m)}(k\boldsymbol{r}_1)+T_\ell \mathfrak{n}\sum_{n'}\int_{\mathcal{R}_a}\mathcal{U}_{n'(\ell,m)}(k\boldsymbol{r}_1-k\boldsymbol{r}_2)\langle f_{n'}\rangle(\boldsymbol{r}_2,\boldsymbol{r}_1)\,\mathrm{d}\boldsymbol{r}_2\\ +T_\ell \mathfrak{n}\sum_{n'}\mathcal{K}_{n'(\ell,m)}(\boldsymbol{r}_1).\end{aligned} \tag{7.3}$$

In [9, eqn (4.6)], all the terms above, except $\mathcal{K}_{n'(\ell,m)}(\boldsymbol{r}_1)$, are greatly simplified using the assumption (7.1). Here we will simplify the extra term $\mathcal{K}_{n'(\ell,m)}(\boldsymbol{r}_1)$, which appears because a more general pair-correlation is used.

By changing the variable of integration to $\boldsymbol{r}=\boldsymbol{r}_2-\boldsymbol{r}_1$, we obtain

$$\mathcal{K}_{n'n}(\boldsymbol{r}_1)=\int_{a_{12}}^{b_{12}}\int_0^{2\pi}\mathcal{U}_{n'n}(-k\boldsymbol{r})\langle f_{n'}\rangle(\boldsymbol{r}+\boldsymbol{r}_1)\,\mathrm{d}\Omega\,\delta g(r)r^2\,\mathrm{d}r, \tag{7.4}$$

where we used the solid angle $d\Omega=\sin\theta\,\mathrm{d}\theta\,\mathrm{d}\phi$.

Using (7.1) and the definitions (A 3) we simplify (7.4) to obtain

$$\begin{aligned}\mathcal{K}_{n'n}(\boldsymbol{r}_1)&=\sum_{n_1n_2n_3}(-1)^{\ell_1}c_{n'nn_1}\mathcal{V}_{n_2n_3}(k_\star\boldsymbol{r}_1)F_{n'n_2}\\ &\quad\times\int_{a_{12}}^{b_{12}}\left[\int\mathrm{Y}_{n_1}(\hat{\boldsymbol{r}})\mathrm{Y}_{n_3}(\hat{\boldsymbol{r}})\,\mathrm{d}\Omega\right]\mathrm{h}_{\ell_1}(kr)\mathrm{j}_{\ell_3}(k_\star r)\delta g(r)r^2\,\mathrm{d}r\\ &=\sum_{n_1n_2n_3}c_{nn'n_3}c_{n_1n_2n_3}\mathrm{v}_{n_2}(k_\star\boldsymbol{r}_1)F_{n'n_1}W_{\ell_3},\end{aligned} \tag{7.5}$$

where W_{ℓ_3} is defined by (3.18), and again we use the notation $n_j=(\ell_j,m_j)$.

Because $\mathrm{v}_{n_2}(k_\star\boldsymbol{r}_1)$ is the only term on the right-hand side that depends on $\boldsymbol{r}_1$, we conclude that $\mathcal{K}_{n'n}(\boldsymbol{r}_1)$ satisfies $\nabla^2\mathcal{K}_{n'n}(\boldsymbol{r}_1)=-k_\star^2\mathcal{K}_{n'n}(\boldsymbol{r}_1)$. Using this in [9, eqn (4.6)] leads us to modify that equation to

$$\boxed{F_{nn_2}+T_\ell\sum_{n_1n'}G_{nn_2,n_1n'}F_{n'n_1}=0,}\quad\text{(the regular eigensystem)}, \tag{7.6}$$

where

$$G_{nn_2,n_1n'}=\mathfrak{n}\sum_{n_1n_3n'}c_{nn'n_3}c_{n_1n_2n_3}\mathrm{K}_{\ell_3}, \tag{7.7}$$

and K_ℓ is defined by (3.16).

(a) Spherical symmetry

The governing system (7.6) is valid for any incident wave, and does not make any assumptions of symmetry. By assuming spherical symmetry, we can greatly simplify this system.

If we assume that the incident wave is spherically symmetric, and that the particles are distributed isotropically, then the whole system becomes spherically symmetric. To that end, we consider the incident wave

$$u_{\text{in}}(\boldsymbol{r}) = \mathrm{v}_0(k\boldsymbol{r}) = \frac{\mathrm{j}_0(kr)}{\sqrt{4\pi}}. \tag{7.8}$$

Then equation (3.2) holds (see appendix D), and combining with (7.1) yields

$$\boxed{F_{nn_2} = \delta_{\ell,\ell_2}\delta_{m,-m_2}(-1)^m F_\ell.} \quad \text{(Spherical symmetry reduction)} \tag{7.9}$$

Substituting the above into (7.6) leads to

$$\delta_{\ell,\ell_2}\delta_{m,-m_2}(-1)^m F_\ell + T_\ell \sum_{n'} G_{nn_2,(\ell',-m)n'}(-1)^{m'} F_{\ell'} = 0, \tag{7.10}$$

where

$$\sum_{m'} G_{nn_2,(\ell',-m)n'}(-1)^{m'} = \mathfrak{n} \sum_{n_3 m'} c_{nn'n_3} c_{(\ell',-m)n_2 n_3}(-1)^{m'} K_{\ell_3}. \tag{7.11}$$

Again, we have used notation of the kind $n = (\ell, m)$ for brevity. Our goal now is to use the orthogonality relation (A 10) to simplify the above. In particular, we use the properties (A 8), (A 11) and (A 12) to reach

$$c_{nn'n_3} c_{(\ell',-m')n_2 n_3}(-1)^{m'} = c_{n_3(\ell',-m')n} c_{n_3(\ell',-m')(\ell_2,-m_2)}(-1)^{\ell_3+m}.$$

Then, using (A 10), we obtain

$$\begin{aligned}\sum_{m_3 m'} c_{n_3(\ell,-m')n} c_{n_3(\ell,-m')(\ell_2,-m_2)} &= 4\pi\,\delta_{\ell,\ell_2}\delta_{m,-m_2}(2\ell_3+1)(2\ell'+1)\begin{pmatrix}\ell_3 & \ell' & \ell\\ 0 & 0 & 0\end{pmatrix}^2 \\ &= \delta_{\ell,\ell_2}\delta_{m,-m_2} c_{(\ell',0)(\ell,0)(\ell_3,0)} \mathrm{i}^{-\ell'+\ell+\ell_3}\sqrt{\frac{4\pi(2\ell_3+1)(2\ell'+1)}{2\ell+1}}.\end{aligned} \tag{7.12}$$

Defining $S_\ell = \mathrm{i}^{-\ell}\sqrt{2\ell+1}F_\ell$, and substituting the above into (7.11) and (7.10) leads to the dispersion equation (3.14).

The effective wavenumber $k_\star$ and a basis for the vectors F_ℓ are obtained from the dispersion equation (3.14). To fully determine the solution, we make use of [9, eqn (6.3)], which is like a boundary condition. In particular, using (7.9) in [9, eqn (6.3)] leads to

$$\delta_{m_2,-m} \sum_{n' n_3} c_{n'n_3 n} c_{n'n_3(\ell_2,m)}(-1)^{m+\ell_3} Z_{\ell'} = c_{(0,0)nn_2} A_{\text{in}}, \tag{7.13}$$

where we used the properties (A 8), (A 11) and (A 12), together with $g_n = \delta_{n,0}A_{\text{in}}$, which comes from comparing the incident field term in [9, eqn (3.17)] with (2.5). The components $Z_{\ell'}$ are given by [9, eqn (6.4)]:

$$Z_{\ell'} = \frac{R-a}{k^2-k_\star^2}\mathrm{N}_{l'}(kR-ka, k_\star R - k_\star a)F_{\ell'}\mathfrak{n}. \tag{7.14}$$

Using the orthogonality property (7.12), followed by (A 6), we can rewrite (7.13) in the form

$$\sum_{\ell' \ell_3} c_{(\ell_3,0)(\ell,0)(\ell',0)} \mathrm{i}^{-\ell_3+\ell+\ell'} \frac{\sqrt{4\pi(2\ell_3+1)(2\ell'+1)}}{\sqrt{2\ell+1}}(-1)^{\ell_3} Z_{\ell'} = \sqrt{4\pi}(-1)^\ell A_{\text{in}}. \tag{7.15}$$

Finally, we use the orthogonality relation [25, eqn (3.7.7)] to write

$$\sum_{\ell_3} c_{(\ell_3,0),(\ell,0),(\ell',0)} \mathrm{i}^{\ell+\ell'-\ell_3} \frac{\sqrt{4\pi(2\ell_3+1)(2\ell'+1)}}{\sqrt{2\ell+1}}(-1)^{\ell_3} = 4\pi(2\ell'+1)(-1)^{\ell+\ell'}, \tag{7.16}$$

which when substituted into (7.15) leads to (3.20).

8. Conclusion

This work lays the foundation for a complete numerical validation of effective wave theories for particulate materials. By numerical validation, we mean using full Monte Carlo simulations and then comparing the results with theoretical predictions, which have so far been extremely challenging [11–14]. To overcome this challenge, we provide methods to calculate the ensemble average scattering from a finite sphere filled with particles, which is accurate for broad frequency range and volume fractions. Theoretical predictions for a finite sphere are far easier to verify with Monte Carlo methods.

(a) Two theoretical methods

In this work, we provide two methods to calculate the ensemble average wave scattered from a particulate material within a sphere that is excited by a spherically symmetric source. The first method is called the Integral method and is given in §3a. It only makes use of the Quasi-Crystalline approximation (QCA). The second method is called the Effective wave method, given in §3b, and it further assumes that only one effective wave and wavenumber is excited. By imposing spherical symmetry the methods are greatly simplified and are therefore easy to evaluate, change the particle pair-correlation, and do parameter sweeps. The bulk of this paper provides the proofs needed to establish both these methods in §§5–7.

(b) Validating effective wavenumbers

At first it may appear that the scenario of spherical symmetry is a very specific case that is difficult to relate to the more useful scenarios of plane wave incident on a plate filled with particles. However, we showed in this work that the same effective wavenumbers appear for both the spherical symmetry case and the cases of plane wave incidence on a plate. This means that numerically validating the methods for spherical symmetry also serves as a validation of the prediction of the effective wavenumbers for all cases, see [9] for details. The effective wavenumbers are often the most important features to numerically validate, as many experimental methods are based on the effective wavenumbers [37–39].

Future directions. One clear next direction is to use Monte-Carlo simulations, which are computationally more intense, to validate the methods provided here for particles within a sphere. Such a validation could be the first broad frequency range, and highly accurate, validation of effective wave theory and of the Quasi-Crystalline Approximation (QCA) which is the only approximation used to reach the Integral method shown in §3a. To achieve this, one could simulate the scattering from a finite number of particles within a sphere, and repeat this many times for different particles configurations, where the average scattering from every configuration could be compared to the theoretical methods presented here. Achieving this type of numerical validation would be an important step forward in the field: it would indicate what frequency ranges, and particle pair-correlations, can be used in effective theory. In turn this will inform where the theory can be used for both characterization and design of disordered particulate materials.

Data accessibility. The software for both the Effective waves and Integral method deduced in this paper is available at [23,40]. Examples are given in https://juliawavescattering.github.io/EffectiveWaves.jl/dev/manual/sphere/.

Declaration of AI use. We have not used AI-assisted technologies in creating this article.

Authors' contributions. A.L.G.: conceptualization, formal analysis, methodology, project administration, software, visualization, writing—original draft, writing—review and editing; S.H.: data curation, methodology, software, visualization, writing—review and editing; G.K.: formal analysis, methodology, writing—review and editing.

All authors gave final approval for publication and agreed to be held accountable for the work performed therein.

Conflict of interest declaration. We declare we have no competing interests.

Funding. A.L.G. funded by EPSRC (EP/V012436/1) to support this work, and travel funding from UKAN (EP/V007866/1).

Acknowledgements. A.L.G. gratefully acknowledges funding from EPSRC (EP/V012436/1) to support this work, and travel funding from UKAN (EP/V007866/1). All acknowledge the Isaac Newton Institute for Mathematical Sciences for support and hospitality during the programme Mathematical Theory and Applications of Multiple Wave Scattering, which was supported by the EPSRC (EP/R014604/1) and the Simons Foundation.

Appendix A. Translation matrices

The translation properties of the spherical waves are instrumental for the formulation and the solution of the scattering problem of many individual particles. These translation properties are well known, and we refer to, e.g. [41,42] for details. Some of their properties are reviewed in this appendix.

Let $\boldsymbol{r}' = \boldsymbol{r} + \boldsymbol{d}$, then the translation matrices for a translation $\boldsymbol{d}$ are [41]

$$\left.\begin{aligned} \mathrm{v}_n(k\boldsymbol{r}') &= \sum_{n'} \mathcal{V}_{nn'}(k\boldsymbol{d})\mathrm{v}_{n'}(k\boldsymbol{r}), \quad \text{for all } \boldsymbol{d}, \\ \mathrm{u}_n(k\boldsymbol{r}') &= \sum_{n'} \mathcal{V}_{nn'}(k\boldsymbol{d})\mathrm{u}_{n'}(k\boldsymbol{r}), \quad |\boldsymbol{r}| > |\boldsymbol{d}| \\ \text{and} \qquad \mathrm{u}_n(k\boldsymbol{r}') &= \sum_{n'} \mathcal{U}_{nn'}(k\boldsymbol{d})\mathrm{v}_{n'}(k\boldsymbol{r}), \quad |\boldsymbol{r}| < |\boldsymbol{d}| \end{aligned}\right\}. \tag{A 1}$$

Translation in the opposite direction is identical to the Hermitian conjugate of the translation matrices [43], i.e.

$$\mathcal{V}_{nn'}(-k\boldsymbol{d}) = \mathcal{V}^*_{n'n}(k^*\boldsymbol{d}) = (-1)^{\ell-\ell'}\mathcal{V}_{nn'}(k\boldsymbol{d}), \quad \mathcal{U}_{nn'}(-k\boldsymbol{d}) = (-1)^{\ell-\ell'}\mathcal{U}_{nn'}(k\boldsymbol{d}). \tag{A 2}$$

The translation matrix $\mathcal{V}_{nn'}(k\boldsymbol{d})$ is identical to $\mathcal{U}_{nn'}(k\boldsymbol{d})$ but with $\mathrm{h}^{(1)}_\lambda(k|\boldsymbol{d}|)$ replaced with $\mathrm{j}_\lambda(k|\boldsymbol{d}|)$.

Notice that the translation matrices $\mathcal{V}_{nn'}(k\boldsymbol{d})$ and $\mathcal{U}_{nn'}(k\boldsymbol{d})$ have the form

$$\mathcal{V}_{nn'}(k\boldsymbol{d}) = \sum_{n_1} c_{nn'n_1}\mathrm{v}_{n_1}(k\boldsymbol{d}) \quad \text{and} \quad \mathcal{U}_{nn'}(k\boldsymbol{d}) = \sum_{n_1} \mathrm{c}_{nn'n_1}\mathrm{u}_{n_1}(k\boldsymbol{d}), \tag{A 3}$$

where the summation over the multi-index $n_1 = \{\ell_1, m_1\}$ effectively is over $|\ell - \ell'| \le \ell_1 \le \ell + \ell'$, and $m_1 = m - m'$. The explicit values of the coefficients $c_{nn'n_1}$ are

$$\mathrm{c}_{nn'n_1} = 4\pi \mathrm{i}^{\ell'-\ell+\ell_1} \int_\Omega \mathrm{Y}_n(\theta,\phi)\mathrm{Y}^*_{n'}(\theta,\phi)\mathrm{Y}^*_{n_1}(\theta,\phi)\,\sin\theta\,\mathrm{d}\theta\,\mathrm{d}\phi. \tag{A 4}$$

From this definition, together with Unsöld's theorem [44]

$$\sum_{m=-\ell}^{\ell} \mathrm{Y}^*_{(\ell,m)}(\theta,\phi)\mathrm{Y}_{(\ell,m)}(\theta,\phi) = \frac{2\ell+1}{4\pi},$$

and the orthogonality of the spherical harmonics it can be shown that

$$\sum_{m'} \mathrm{c}_{nn'(\ell',-m')}(-1)^{m'} = \sqrt{4\pi}\mathrm{i}^{2\ell'-\ell}\delta_{n,0}(2\ell'+1) \tag{A 5}$$

and

$$\mathrm{c}_{(0,0)nn_2} = \sqrt{4\pi}(-1)^{\ell+m}\delta_{m_2,-m}\delta_{\ell_2,\ell}. \tag{A 6}$$

The coefficients $\mathrm{c}_{nn'n_1}$ can also be written in terms of the Wigner 3-j symbol [25, (4.6.3), p. 63] in the form

$$\mathrm{c}_{nn'n''} = \mathrm{i}^{\ell'-\ell+\ell''}(-1)^m\sqrt{4\pi(2\ell+1)(2\ell'+1)(2\ell''+1)}\begin{pmatrix}\ell & \ell' & \ell'' \\ 0 & 0 & 0\end{pmatrix}\begin{pmatrix}\ell & \ell' & \ell'' \\ m & -m' & -m''\end{pmatrix}. \tag{A 7}$$

Note that the coefficients $c_{nn'n''}$ are all real due to orthogonality in the azimuthal variable. Further the $c_{nn'n''}$ are only non-zero when

$$m - m' = m'', \quad |\ell - \ell'| \leq \ell'' \leq \ell + \ell', \quad \ell + \ell' + \ell'' = \text{even integer}, \tag{A 8}$$

and should only be evaluated for $\ell, \ell', \ell'' \geq 0$ and

$$-\ell \leq m \leq \ell, \quad -\ell' \leq m' \leq \ell', \quad -\ell'' \leq m'' \leq \ell''. \tag{A 9}$$

The Wigner 3j have the following orthogonality relation:

$$(2\ell_3 + 1) \sum_{m_1 m_2} \begin{pmatrix} \ell_1 & \ell_2 & \ell_3 \\ m_1 & m_2 & m_3 \end{pmatrix} \begin{pmatrix} \ell_1 & \ell_2 & \ell_3' \\ m_1 & m_2 & m_3' \end{pmatrix} = \delta_{\ell_3,\ell_3'} \delta_{m_3,m_3'} \{\ell_1 \ell_2 \ell_3\}, \tag{A 10}$$

where $\{\ell_1 \ell_2 \ell_3\}$ is the triangular delta.

The special case $c_{nn(0,0)} = \sqrt{4\pi}$ and the following properties are useful:

$$c_{nn'n''} = c_{nn''n'} = c_{(\ell,-m)(\ell',-m')(\ell'',-m'')}, \tag{A 11}$$

$$c_{nn'n''} = (-1)^{m''+\ell''} c_{n'n(\ell'',-m'')} = (-1)^{\ell'+m'} c_{n''(\ell',-m')n} \tag{A 12}$$

and

$$\sum_{n_1} \mathrm{i}^{\ell_1} Y_{n_1}(\theta,\phi) c_{n_1 n' n} = 4\pi \mathrm{i}^{\ell+\ell'} Y_n(\theta,\phi) Y_{n'}(\theta,\phi), \tag{A 13}$$

where the last is the contraction rule, or the linearization formula [45]. For real θ and ϕ, the linearization formula can be deduced by multiplying both sides of (A 13) by $Y^*_{n_2}(\hat{\boldsymbol{r}})$, then integrating over $\hat{\boldsymbol{r}}$, and applying the definition (A 4).

The Wigner D-matrix are rotation matrices [25], so they satisfy

$$\sum_{m_1=-\ell}^{\ell} D^{\ell}_{m_3 m_1}(\alpha,\beta,\gamma)(D^{\ell}_{m_2 m_1}(\alpha,\beta,\gamma))^* = \delta_{m_3,m_2}, \tag{A 14}$$

because the $D^{\ell}_{m_3 m_1}$ are rotation matrices. Note that the complex conjugate $(D^{\ell}_{m_2 m_1})^* = (-1)^{-m_1-m_2} D^{\ell}_{(-m_2)(-m_1)}$.

Integrating over the Euler angles leads to the useful identities

$$\frac{1}{8\pi^2} \int_0^{2\pi} \int_0^{\pi} \int_0^{2\pi} D^{\ell_3}_{m_3 m_1}(\alpha,\beta,\gamma) D^{\ell}_{mm'}(\alpha,\beta,\gamma) \sin\beta \, \mathrm{d}\alpha \, \mathrm{d}\beta \, \mathrm{d}\gamma = \delta_{m,-m_3} \delta_{m',-m_1} \delta_{\ell,\ell_3} \frac{(-1)^{m_1+m_3}}{2\ell+1}, \tag{A 15}$$

and

$$\frac{1}{8\pi^2} \int_0^{2\pi} \int_0^{\pi} \int_0^{2\pi} D^{\ell_1}_{m_1 m_1'} D^{\ell_2}_{m_2 m_2'} D^{\ell_3}_{m_3 m_3'} \sin\beta \, \mathrm{d}\alpha \, \mathrm{d}\beta \, \mathrm{d}\gamma = \begin{pmatrix} \ell_1 & \ell_2 & \ell_3 \\ m_1 & m_2 & m_3 \end{pmatrix} \begin{pmatrix} \ell_1 & \ell_2 & \ell_3 \\ m_1' & m_2' & m_3' \end{pmatrix}, \tag{A 16}$$

which are equation (4.6.1) and (4.6.2) from [25].

Appendix B. Prove rotated incident wave

Here we prove that

$$\sum_{m=-\ell}^{\ell} D^{\ell}_{m''m} \mathcal{V}_{(0,0)n}(k\mathbf{R}\boldsymbol{r}_1) = \mathcal{V}_{(0,0)(\ell,m'')}(k\boldsymbol{r}_1). \tag{B 1}$$

Using definition (A 3), and properties (A 11) and (A 12), we have

$$\mathcal{V}_{(0,0)n}(k\mathbf{R}\boldsymbol{r}_1) = \sum_{n_1} c_{(0,0)nn_1} v_{n_1}(k\mathbf{R}\boldsymbol{r}_1) = \sum_{n_1} c_{(0,0)nn_1} \sum_{m_2} v_{(\ell_1,m_2)}(k\boldsymbol{r}_1) D^{\ell_1}_{m_2 m_1}(\alpha,\beta,\gamma). \tag{B 2}$$

Next we use $c_{(0,0)n(\ell_1,m_1)} = \sqrt{4\pi}(-1)^{\ell+m}\delta_{m_1,-m}\delta_{\ell_1,\ell}$, which follows from (A 4), in the above to obtain

$$\sum_{m=-\ell}^{\ell} D^{\ell}_{m''m}\mathcal{V}_{(0,0)(\ell,m)}(k\mathbf{P}\boldsymbol{r}_1) = \sqrt{4\pi}(-1)^{\ell}\sum_{m_2} v_{(\ell,m_2)}(k\boldsymbol{r}_1)\sum_{m=-\ell}^{\ell} D^{\ell}_{m''m}(-1)^{m}D^{\ell}_{m_2(-m)}. \tag{B 3}$$

By writing: $(-1)^{m}D^{\ell}_{m_2(-m)} = (-1)^{m_2}D^{\ell *}_{(-m_2)m}$, we can use

$$\sum_{m=-\ell}^{\ell} D^{\ell}_{m''m}(-1)^{m}D^{\ell}_{m_2(-m)} = (-1)^{m_2}\delta_{m'',-m_2},$$

because the $D^{\ell}_{m_1m_2}$ are rotation matrices. Substituting the above into (B 3) completes the proof of (B 1) because

$$\sum_{m=-\ell}^{\ell} D^{\ell}_{m''m}\mathcal{V}_{(0,0)(\ell,m)}(k\mathbf{P}\boldsymbol{r}_1) = \sqrt{4\pi}(-1)^{\ell+m''}v_{(\ell,-m'')}(k\boldsymbol{r}_1) = \mathcal{V}_{(0,0)(\ell,m'')}(k\boldsymbol{r}_1). \tag{B 4}$$

Appendix C. Prove rotated integral term

Here we prove that, for any square integrable function h, under the assumptions of theorem 5.3, we have

$$\sum_{m'=-\ell'}^{\ell'}\sum_{m=-\ell}^{\ell} D^{\ell}_{m''m}K_{(\ell',m')(\ell,m)}[h_{(\ell',m')}](\mathbf{P}\boldsymbol{r}_1) = \sum_{m'=-\ell'}^{\ell'} K_{(\ell',m')(\ell,m'')}[h^{\mathbf{P}}_{(\ell',m')}](\boldsymbol{r}_1). \tag{C 1}$$

Expanding the left-hand side using (5.16), followed by a change of variables $\boldsymbol{r}_2 \mapsto \mathbf{P}\boldsymbol{r}_2$, and using the invariance of $\mathfrak{n}$ and g under rotations, gives

$$\begin{aligned}
&\sum_{m'=-\ell'}^{\ell'}\sum_{m=-\ell}^{\ell} D^{\ell}_{m''m}K_{(\ell',m')(\ell,m)}[h_{(\ell',m')}](\mathbf{P}\boldsymbol{r}_1)\\
&\quad= \sum_{(\ell_1,m_1)}\sum_{m'=-\ell'}^{\ell'}\sum_{m=-\ell}^{\ell}\sum_{m_2=-\ell_1}^{\ell_1}\int_{\mathcal{R}} D^{\ell}_{m''m}D^{\ell_1}_{m_2m_1}c_{(\ell',m')(\ell,m)(\ell_1,m_1)}u_{(\ell_1,m_2)}(k\boldsymbol{r}_1 - k\boldsymbol{r}_2)\\
&\qquad\times h_{(\ell',m')}(\mathbf{P}\boldsymbol{r}_2,\mathbf{P}\boldsymbol{r}_1)g(\boldsymbol{r}_1,\boldsymbol{r}_2)\mathfrak{n}(\boldsymbol{r}_2)\,\mathrm{d}\boldsymbol{r}_2,
\end{aligned} \tag{C 2}$$

where we used (A 3) and (5.2) to substitute

$$\begin{aligned}
\mathcal{U}_{(\ell',m')(\ell,m)}(k\mathbf{P}(\boldsymbol{r}_1-\boldsymbol{r}_2)) &= \sum_{(\ell_1,m_1)} c_{(\ell',m')(\ell,m)(\ell_1,m_1)}u_{(\ell_1,m_1)}(\mathbf{P}(\boldsymbol{r}_1-\boldsymbol{r}_2))\\
&= \sum_{(\ell,m)} c_{(\ell',m')(\ell,m)(\ell_1,m_1)}\sum_{m_2=-\ell_1}^{\ell_1} u_{(\ell_1,m_2)}(k\boldsymbol{r}_1 - k\boldsymbol{r}_2)D^{\ell_1}_{m_2m_1}.
\end{aligned} \tag{C 3}$$

We can show that the term on the right of (C 1) equals (C 2) by opening it to obtain:

$$\begin{aligned}
\sum_{m'=-\ell'}^{\ell'} K_{n'(\ell,m'')}[h^{\mathbf{P}}_{n'}](\boldsymbol{r}_1) &= \sum_{n_2}\sum_{m'=-\ell'}^{\ell'}\sum_{m_1=-\ell'}^{\ell'}\int_{\mathcal{R}} D^{\ell'}_{m'm_1}c_{(\ell',m')(\ell,m'')n_2}u_{n_2}(k\boldsymbol{r}_1 - k\boldsymbol{r}_2)\\
&\quad\times h_{(\ell',m_1)}(\mathbf{P}\boldsymbol{r}_2,\mathbf{P}\boldsymbol{r}_1)g(\boldsymbol{r}_1,\boldsymbol{r}_2)\mathfrak{n}(\boldsymbol{r}_2)d\boldsymbol{r}_2\\
&= \sum_{(\ell_1,m_1)}\sum_{m'=-\ell'}^{\ell'}\sum_{m=-\ell}^{\ell}\sum_{m_2=-\ell_1}^{\ell_1}\int_{\mathcal{R}} D^{\ell}_{m''m}D^{\ell_1}_{m_2m_1}c_{(\ell',m')(\ell,m)(\ell_1,m_1)}u_{(\ell_1,m_2)}(k\boldsymbol{r}_1 - k\boldsymbol{r}_2)\\
&\quad\times h_{(\ell',m')}(\mathbf{P}\boldsymbol{r}_2,\mathbf{P}\boldsymbol{r}_1)g(\boldsymbol{r}_1,\boldsymbol{r}_2)\mathfrak{n}(\boldsymbol{r}_2)\,\mathrm{d}\boldsymbol{r}_2,
\end{aligned} \tag{C 4}$$

as required, where in the first line we used (A 3), and in the second line we used

$$\sum_{m'=-\ell'}^{\ell'} \mathrm{D}^{\ell'}_{m'm_1} \mathrm{c}_{n'(\ell,m'')n_2} = \sum_{m=-\ell}^{\ell} \sum_{m'=-\ell_2}^{\ell_2} \mathrm{D}^{\ell}_{m''m} \mathrm{D}^{\ell_2}_{m_2m'} \mathrm{c}_{(\ell,m_1)n(\ell_2,m')}, \tag{C 5}$$

which follows from the identity

$$\sum_{m'} \sum_{m=-\ell}^{\ell} \sum_{m_1=-\ell_2}^{\ell_2} \mathrm{c}_{n'n(\ell_2,m_1)} (-1)^{m'} \mathrm{D}^{\ell'}_{m_3(-m')} \mathrm{D}^{\ell}_{m''m} \mathrm{D}^{\ell_2}_{m_2m_1} = \mathrm{c}_{(\ell',-m_3)(\ell,m'')n_2} (-1)^{m_3}, \tag{C 6}$$

after multiplying both sides by $(-1)^{m_3} \mathrm{D}^{\ell'}_{-m_3(m_4)}$ and summing over m_3, and using the orthogonality property (A 14). The above identity (C 6) is obtained by combining equations (4.1.12), (4.2.5) and (4.3.3) from [25], together with definition (A 7).

Appendix D. Proof of the representation (3.2)

Here we use theorems 5.1 and 5.3 to prove the representation (3.2). Let $h(\boldsymbol{r}_1, \boldsymbol{r}_2) := \sum_n \mathrm{Y}_n(\hat{\boldsymbol{r}}_2) \langle f_n \rangle(\boldsymbol{r}_1)$. From theorem 5.3 and definition (5.2) we find that

$$\begin{aligned} h(\boldsymbol{r}_1, \boldsymbol{r}_2) &= \sum_{(\ell,m)} \sum_{m'=-\ell}^{\ell} \mathrm{Y}_{(\ell,m)}(\hat{\boldsymbol{r}}_2) \mathrm{D}^{\ell}_{mm'} \langle f_{(\ell,m')} \rangle(\mathbf{P}\boldsymbol{r}_1) \\ &= \sum_{\ell} \sum_{m'=-\ell}^{\ell} \mathrm{Y}_{(\ell,m')}(\mathbf{P}\hat{\boldsymbol{r}}_2) \langle f_{(\ell,m')} \rangle(\mathbf{P}\boldsymbol{r}_1) = h(\mathbf{P}\boldsymbol{r}_1, \mathbf{P}\boldsymbol{r}_2). \end{aligned} \tag{D 1}$$

From theorem 5.1, we have

$$h(\boldsymbol{r}_1, \boldsymbol{r}_2) = \sum_{(\ell,m)} h_{(\ell,0)(\ell,0)}(r_1) \mathrm{Y}^*_{(\ell,m)}(\hat{\boldsymbol{r}}_1) \mathrm{Y}_{(\ell,m)}(\hat{\boldsymbol{r}}_2),$$

which, when compared with $h(\boldsymbol{r}_1, \boldsymbol{r}_2) := \sum_n \mathrm{Y}_n(\hat{\boldsymbol{r}}_2) \langle f_n \rangle(\boldsymbol{r}_1)$, leads to the representation (3.2).

Appendix E. Proof of the representation (3.3)

Here we use theorems 5.2 and 5.3 to prove the representation (3.3). Let $h(\boldsymbol{r}_1, \boldsymbol{r}_2, \boldsymbol{r}_3) := \sum_n \mathrm{Y}_n(\hat{\boldsymbol{r}}_3) \langle f_n \rangle(\boldsymbol{r}_1, \boldsymbol{r}_2)$. From theorem 5.3, we find that, similar to the two-argument case in the section above,

$$h(\boldsymbol{r}_1, \boldsymbol{r}_2, \boldsymbol{r}_3) = h(\mathbf{P}\boldsymbol{r}_1, \mathbf{P}\boldsymbol{r}_2, \mathbf{P}\boldsymbol{r}_3). \tag{E 1}$$

From theorem 5.2 and the properties (A 11) we obtain

$$\begin{aligned} h(\boldsymbol{r}_1, \boldsymbol{r}_2, \boldsymbol{r}_3) = &\sum_{\substack{(\ell_1,m_1) \\ (\ell_2,m_2)}} \sum_{(\ell_3,m_3)} h_{(\ell_1,0)(\ell_2,0)(\ell_3,0)}(r_1, r_2) \frac{\mathrm{c}_{(\ell_1,m_1)(\ell_2,m_2)(\ell_3,m_3)}}{\mathrm{c}_{(\ell_1,0)(\ell_2,0)(\ell_3,0)}} \\ &\times \mathrm{Y}_{(\ell_1,m_1)}(\hat{\boldsymbol{r}}_1) \mathrm{Y}^*_{(\ell_2,m_2)}(\hat{\boldsymbol{r}}_2) \mathrm{Y}^*_{(\ell_3,m_3)}(\hat{\boldsymbol{r}}_3), \end{aligned}$$

Comparing the above with the definition of h leads to the representation (3.3).

Appendix F. Reducing the integral term

In §6, we need the identity (F 4), where we used the shorthand (5.16). We can easily reduce this term by using (C 1) and $\langle f^{\mathbf{P}}_n \rangle(\boldsymbol{r}_2, \boldsymbol{r}_1) = \langle f_n \rangle(\boldsymbol{r}_2, \boldsymbol{r}_1)$.

Assume we have some field that satisfies $\langle f_n^{\mathbf{P}}\rangle(\boldsymbol{r}_2,\boldsymbol{r}_1)=\langle f_n\rangle(\boldsymbol{r}_2,\boldsymbol{r}_1)$ for every rotation $\mathbf{P}$, substituting this field into (C 1) leads to

$$\sum_{m'=-\ell'}^{\ell'} K_{n'n}[\langle f_{n'}\rangle](\boldsymbol{r}_1)=\sum_{m''=-\ell}^{\ell}\mathrm{D}^{\ell}_{mm''}\sum_{m'=-\ell'}^{\ell'} K_{n'(\ell,m'')}[\langle f_{n'}\rangle](\mathbf{P}\boldsymbol{r}_1), \tag{F 1}$$

where we swapped m and m'' for every rotation matrix $\mathbf{P}$. We can rewrite this by defining

$$k_{\ell'}(\boldsymbol{r}_1,\boldsymbol{r}_2):=\sum_{n}\sum_{m'=-\ell'}^{\ell'} K_{n'n}[\langle f_{n'}\rangle](\boldsymbol{r}_1)\mathrm{Y}_n(\hat{\boldsymbol{r}}_2), \tag{F 2}$$

and multiplying both sides of (F 1) by $\mathrm{Y}_n(\hat{\boldsymbol{r}}_2)$ and summing over n to obtain

$$k_{\ell'}(\boldsymbol{r}_1,\boldsymbol{r}_2)=k_{\ell'}(\mathbf{P}\boldsymbol{r}_1,\mathbf{P}\boldsymbol{r}_2), \tag{F 3}$$

where we used (5.2) on the right side. The above lets us use theorem 5.1 to write

$$k_{\ell'}(\boldsymbol{r}_1,\boldsymbol{r}_2)=\sum_{n} k_{\ell'\ell}(r_1)\mathrm{Y}^*_n(\hat{\boldsymbol{r}}_1)\mathrm{Y}_n(\hat{\boldsymbol{r}}_2),$$

where $k_{\ell'\ell}$ is a function which depends only on ℓ' and ℓ. Comparing the above with (F 2), and using the orthogonality of the spherical harmonics, leads us to

$$\sum_{m'=-\ell'}^{\ell'} K_{n'n}[\langle f_{n'}\rangle](\boldsymbol{r}_1)=k_{\ell'\ell}(r_1)\mathrm{Y}^*_n(\hat{\boldsymbol{r}}_1). \tag{F 4}$$

To reach the version of this identity we need we multiply both sides by $\mathrm{Y}_{n_0}(\hat{\boldsymbol{r}}_1)$, integrate over the solid angle $d\Omega_1$, and sum over ℓ' to obtain

$$\int\sum_{n'} K_{n'n}[\langle f_{n'}\rangle](\boldsymbol{r}_1)\mathrm{Y}_{n_0}(\hat{\boldsymbol{r}}_1)\mathrm{d}\Omega_1=k_{\ell}(r_1)\delta_{n,n_0}, \tag{F 5}$$

where $k_\ell(r_1):=\sum_{\ell'}k_{\ell'\ell}(r_1)$.

References

1. Merkus HG, Meesters GM. 2013 *Particulate products: tailoring properties for optimal performance*, vol. 19. Berlin, Germany: Springer.
2. Mishchenko MI, Travis LD, Lacis AA. 2006 *Multiple scattering of light by particles: radiative transfer and coherent backscattering*. Cambridge, UK: Cambridge University Press.
3. Lax M. 1951 Multiple scattering of waves. *Rev. Mod. Phys.* **23**, 287. (doi:10.1103/RevModPhys.23.287)
4. Vynck K, Pierrat R, Carminati R, Froufe-Pérez LS, Scheffold F, Sapienza R, Vignolini S, Sáenz JJ. 2021 Light in correlated disordered media. (http://arxiv.org/abs/2106.13892)
5. Tsang L, Kong JA, Ding KH. 2000 *Scattering of electromagnetic waves: theories and applications*. New York, NY: John Wiley & Sons.
6. Tsang L, Kong JA, Ding KH, Ao CO. 2001 *Scattering of electromagnetic waves: numerical simulations*. New York, NY: John Wiley & Sons.
7. Tsang L, Kong JA. 2001 *Scattering of electromagnetic waves: advanced topics*. New York, NY: John Wiley & Sons.
8. Linton CM, Martin PA. 2006 Multiple scattering by multiple spheres: a new proof of the Lloyd–Berry formula for the effective wavenumber. *SIAM J. Appl. Math.* **66**, 1649–1668. (doi:10.1137/050636401)
9. Gower AL, Kristensson G. 2021 Effective waves for random three-dimensional particulate materials. *New J. Phys.* **23**, 063083. (doi:10.1088/1367-2630/abdfee)
10. Willis J. 2020 Transmission and reflection at the boundary of a random two-component composite. *Proc. R. Soc. A* **476**, 20190811. (doi:10.1098/rspa.2019.0811)
11. Chekroun M, Le Marrec L, Lombard B, Piraux J, Abraham O. 2009 Comparison between a multiple scattering method and direct numerical simulations for elastic wave propagation

in concrete. In *Ultrasonic wave propagation in non homogeneous media* (eds A Leger, M Deschamps), pp. 317–327. Berlin, Germany: Springer.
12. Chekroun M, Le Marrec L, Lombard B, Piraux J. 2012 Time-domain numerical simulations of multiple scattering to extract elastic effective wavenumbers. *Waves in Random and Complex Media* **22**, 398–422. (doi:10.1080/17455030.2012.704432)
13. Gower AL, Gower RM, Deakin J, Parnell WJ, Abrahams ID. 2018 Characterising particulate random media from near-surface backscattering: a machine learning approach to predict particle size and concentration. *Europhys. Lett.* **122**, 54001. (doi:10.1209/0295-5075/122/54001)
14. Muinonen K, Mishchenko M, Dlugach J, Zubko E, Penttilä A, Videen G. 2012 Coherent backscattering verified numerically for a finite volume of spherical particles. *Astrophys. J.* **760**, 118. (doi:10.1088/0004-637X/760/2/118)
15. Gower AL, Smith MJA, Parnell WJ, Abrahams ID. 2018 Reflection from a multi-species material and its transmitted effective wavenumber. *Proc. R. Soc. A* **474**, 20170864. (doi:10.1098/rspa.2017.0864)
16. Ganesh M, Hawkins SC. 2017 Algorithm 975: TMATROM–a t-matrix reduced order model software. *ACM Trans. Math. Softw.* **44**, 901–918. (doi:10.1145/3054945)
17. Gower AL, Abrahams ID, Parnell WJ. 2019 A proof that multiple waves propagate in ensemble-averaged particulate materials. *Proc. R. Soc. A* **475**, 20190344. (doi:10.1098/rspa.2019.0344)
18. Sgrignuoli F, Torquato S, Dal Negro L. 2022 Subdiffusive wave transport and weak localization transition in three-dimensional stealthy hyperuniform disordered systems. *Phys. Rev. B* **105**, 064204. (doi:10.1103/PhysRevB.105.064204)
19. Gkantzounis G, Amoah T, Florescu M. 2017 Hyperuniform disordered phononic structures. *Phys. Rev. B* **95**, 094120. (doi:10.1103/PhysRevB.95.094120)
20. Leseur O, Pierrat R, Carminati R. 2016 High-density hyperuniform materials can be transparent. *Optica* **3**, 763–767. (doi:10.1364/OPTICA.3.000763)
21. Rowley WD, Parnell WJ, Abrahams ID, Voisey SR, Lamb J, Etaix N. 2018 Deepening subwavelength acoustic resonance via metamaterials with universal broadband elliptical microstructure. *Appl. Phys. Lett.* **112**, 251902. (doi:10.1063/1.5022197)
22. Smith MJ, Abrahams ID. 2022 Tailored acoustic metamaterials. Part I. Thin-and thick-walled Helmholtz resonator arrays. *Proc. R. Soc. A* **478**, 20220124. (doi:10.1098/rspa.2022.0124)
23. Gower A. 2019 EffectiveWaves.jl: a package to calculate ensemble averaged waves in heterogeneous materials. See https://github.com/arturgower/EffectiveWaves.jl. The version used for this paper was https://github.com/JuliaWaveScattering/EffectiveWaves.jl/tree/v0.3.4.
24. Kristensson G. 2015 Coherent scattering by a collection of randomly located obstacles–an alternative integral equation formulation. *J. Quant. Spectrosc. Radiat. Transfer* **164**, 97–108. (doi:10.1016/j.jqsrt.2015.06.004)
25. Edmonds AR. 1974 *Angular momentum in quantum mechanics*, 3rd edn. Princeton, NJ: Princeton University Press.
26. Kristensson G. 2016 *Scattering of electromagnetic waves by obstacles*. Mario Boella Series on Electromagnetism in Information and Communication. Edison, NJ, USA: SciTech Publishing.
27. Mackowski DW, Mishchenko MI. 2011 Direct simulation of multiple scattering by discrete random media illuminated by Gaussian beams. *Phys. Rev. A* **83**, 013804. (doi:10.1103/PhysRevA.83.013804)
28. Gower AL, Deakin J. 2020 MultipleScatering.jl: a Julia library for simulating, processing, and plotting multiple scattering of waves. *Github github.com/JuliaWaveScattering/MultipleScattering.jl*.
29. Ganesh M, Hawkins SC. 2015 An efficient $O(N)$ algorithm for computing $O(N^2)$ acoustic wave interactions in large N-obstacle three dimensional configurations. *BIT* **55**, 117–139. (doi:10.1007/s10543-014-0491-3)
30. Ganesh M, Hawkins SC. 2019 A high order algorithm for multiple scattering from large sound hard three dimensional configurations. *J. Comput. Appl. Math.* **362**, 324–340. (doi:10.1016/j.cam.2018.10.053)
31. Mishchenko MI. 1990 Extinction of light by randomly-oriented non-spherical grains. *Astrophys. Space Sci.* **164**, 1–13. (doi:10.1007/BF00653546)
32. Mishchenko MI, Travis LD, Mackowski DW. 1996 T-matrix computations of light scattering by nonspherical particles: a review. *J. Quant. Spectrosc. Radiat. Transfer* **55**, 535–575. (doi:10.1016/0022-4073(96)00002-7)

33. Gower AL, Parnell WJ, Abrahams ID. 2019 Multiple waves propagate in random particulate materials. *SIAM J. Appl. Math.* **79**, 2569–2592. (doi:10.1137/18M122306X)
34. Karnezis A, Piva PS, Gower AL. 2023 The average transmitted wave in random particulate materials. (http://arxiv.org/abs/2308.06843)
35. Percus JK, Yevick GJ. 1958 Analysis of classical statistical mechanics by means of collective coordinates. *Phys. Rev.* **110**, 1. (doi:10.1103/PhysRev.110.1)
36. Abramowitz M, Stegun IA, Romer RH. 1988 *Handbook of mathematical functions with formulas, graphs, and mathematical tables*. Washington, DC: US Government Printing Office.
37. Hunter TN, Darlison L, Peakall J, Biggs S. 2012 Using a multi-frequency acoustic backscatter system as an in situ high concentration dispersion monitor. *Chem. Eng. Sci.* **80**, 409–418. (doi:10.1016/j.ces.2012.06.038)
38. Challis R, Povey M, Mather M, Holmes A. 2005 Ultrasound techniques for characterizing colloidal dispersions. *Rep. Prog. Phys.* **68**, 1541. (doi:10.1088/0034-4885/68/7/R01)
39. Holmes AK, Challis RE, Wedlock DJ. 1993 A wide bandwidth study of ultrasound velocity and attenuation in suspensions: comparison of theory with experimental measurements. *J. Colloid Interface Sci.* **156**, 261–268. (doi:10.1006/jcis.1993.1109)
40. Gower AL. 2023 EffectiveWaves.jl A Julia package to calculate ensemble averaged waves in heterogeneous materials. See https://doi.org/10.5281/zenodo.8379325. (10.5281/zenodo.8379325)
41. Boström A, Kristensson G, Ström S. 1991 Transformation properties of plane, spherical and cylindrical scalar and vector wave functions. In *Field representations and introduction to scattering* (eds VV Varadan, A Lakhtakia, VK Varadan). Acoustic, Electromagnetic and Elastic Wave Scattering, pp. 165–210. Amsterdam, The Netherlands: Elsevier.
42. Friedman B, Russek J. 1954 Addition theorems for spherical waves. *Quart. Appl. Math.* **12**, 13–23. (doi:10.1090/qam/60649)
43. Peterson B, Ström S. 1973 *T*-matrix for electromagnetic scattering from an arbitrary number of scatterers and representations of E(3). *Phys. Rev. D* **8**, 3661–3678. (doi:10.1103/PhysRevD.8.3661)
44. Unsöld A. 1927 Beiträge zur quantenmechanik der atome. *Annalen der Physik* **387**, 355–393. (doi:10.1002/andp.19273870304)
45. Martin PA. 2006 *Multiple scattering: interaction of time-harmonic waves with n obstacles*, vol. 107. Cambridge, UK: Cambridge University Press.